universität wien

MASTERARBEIT / MASTER'S THESIS

Titel der Masterarbeit / Title of the Master's Thesis

„Contribution of murine uterine aging to delayed parturiton"

verfasst von / submitted by

Stefan Pavloski

angestrebter akademischer Grad / in partial fulfilment of the requirements for the degree of

Master of Science (MSc)

Wien, 2023 / Vienna, 2023

Studienkennzahl lt. Studienblatt / degree programme code as it appears on the student record sheet:	UA 066 220
Studienrichtung lt. Studienblatt / degree programme as it appears on the student record sheet:	Joint-Masterstudium Evolutionary Systems Biology
Betreut von / Supervisor:	Univ.-Prof. Mag. Dr. Mihaela Pavličev

Acknowledgements

My most wholehearted appreciation goes to my Master's thesis advisor Professor Mihaela Pavličev, and my unofficial supervisor Doctor Caitlin McDonough-Goldstein. I am immensely grateful for their time, effort and mentorship that were integral to my success throughout my studies. In addition, I want to acknowledge Severin Bachmayer BSc for collaborating on the Reproductive Aging Project, and Gülay Dagdas, PhD for her technical assistance and emotional support throughout my research. At last, I wish to express my gratitude to everyone in the Pavličev group at the University of Vienna. Because of their encouragement, my time spent studying and living in Vienna has been exceptionally rewarding and memorable.

Contents:

1. Abstract

Aging impacts pregnancy progression and gestational length, leading to complications during parturition, such as dystocia. These phenotypes may arise due to the ovarian senescence, as well as the senescence of the uterine and cervical tissues. Here we investigate the age-related changes in the uterus and cervix that influence timing of parturition with in-depth transcriptional and histological techniques. We compare 3- and 8-months old mice, at 15.5 dpc and 17.5 dpc. Most structural variation in utero-placental unit and cervix are accounted for by the progression of pregnancy, while differences in collagen density in cervical stroma is best accounted for by aging. Moreover, glycogen level in placentas exhibit age-specific patterns, with young mice displaying higher levels of glycogen at 15.7 dpc, which decrease until the later time point of gestation. In contrast, old mice exhibit low glycogen levels already at the earlier time point. Analysis of differentially expressed uterine genes reveals distinct patterns between age-groups. From 15.5 dpc to 17.5 dpc, young mice show upregulation in uterus of genes involved in cell respiration processes, whereas old mice display upregulation of genes associated with hormone metabolism. Both age groups exhibit downregulation of genes involved in cell adhesion and immune response at 17.5 dpc. We also found gene families (*Psg*, *Ceacam* and *Prl*) with contrasting patterns of expression: upregulated in young and downregulated in old mice at 17.5 dpc. With this study we contribute to the understanding of the effects of aging in the complex regulatory mechanisms of initiation of parturition in mice.

2. Zusammenfassung

Die Alterung wirkt sich auf den Verlauf und Dauer der Schwangerschaft aus und führt zu Komplikationen während der Geburt, wie z. B. Dystokie. Diese Phänotypen können durch die Alterung der Eierstöcke sowie die der Gebärmutter- und des Gebärmutterhalsgewebes entstehen. Hier untersuchen wir die altersbedingten Veränderungen in der Gebärmutter und im Gebärmutterhals, die den Zeitpunkt der Geburt beeinflussen, mit transkriptionellen und histologischen Techniken. Wir vergleichen 3- und 8-monatige Mäuse von 15,5 bis 17,5 Trächtigkeitstag. Die meisten strukturellen Veränderungen in der utero-plazentaren Einheit und im Gebärmutterhals werden durch das Fortschreiten der Trächtigkeit erklärt, während die Unterschiede in der Kollagendichte im Gebärmutterhalsstroma durch die Alterung bedingt sind. Darüber hinaus weisen die Glykogenspiegel in der Plazenta altersspezifische Muster auf, wobei junge Mäuse um Tag 15,7 höhere Glykogenwerte aufweisen, die später sinken. Im Gegensatz dazu weisen alte Mäuse bereits zum früheren Zeitpunkt niedrige Glykogenwerte auf. Die Analyse der differenziell exprimierten Gebärmuttergene zeigt unterschiedliche Muster zwischen den Altersgruppen. Von Tag 15,5 bis 17,5 zeigen junge Mäuse im Uterus eine höhere Expression von Genen, die an Zellatmungsprozessen beteiligt sind, während alte Mäuse eine Hochregulierung von Genen aufweisen, die mit dem Hormonstoffwechsel verbunden sind. Beide Altersgruppen weisen eine Herabregulierung von Genen auf, die an der Zelladhäsion und der Immunantwort beteiligt sind, und zwar um Tag 17,5. Wir fanden auch Genfamilien (*Psg*, *Ceacam* und *Prl*) mit gegensätzlichen Expressionsmustern: hochreguliert bei jungen und herunterreguliert bei alten Mäusen um Tag 17,5. Mit dieser Studie tragen wir zum Verständnis der Auswirkungen des Alterungsprozesses auf die komplexen Regulationsmechanismen der Geburtseinleitung bei Mäusen bei.

3. Introduction

The process of aging is characterized by a progressive loss of physiological and structural integrity, caused by changes in metabolism and accumulation of damage during the lifespan of an organism. In mammals, the female reproductive system ages more rapidly, with a decline in function occurring decades prior to other organs. There are multiple plausible causes for reproductive senescence and subsequent infertility. In many species, reproductive senescence is associated with a decrease in both the number and the quality of primordial oocytes in the ovaries (Meldrum, 1993; Crawford & Steiner, 2015). However, aging also influences the progression of pregnancy and the length of gestation, including complications in parturition, such as difficult, abnormal or dysfunctional labor, i.e., dystocia (Zaborski et al., 2009; Patel et al., 2017; Cornelius et al., 2019; Fura, 2022). As many tissues are involved in parturition, dystocia - delayed and difficult labor - can be influenced not only by ovarian senescence, but also by senescence of the uterine and cervical tissues, as well as the factors involved in the communication among these tissues (Meldrum, 1993; Sugimoto et al., 1997; Patel et al., 2017; Yomogita et al., 2022).

Both, genetic predisposition and stochastic damage contribute to the progression of aging as they lead to impaired function, tissue and cellular deterioration, as well as chronic disease (López-Otín et al, 2013; Giller et al., 2020). Thereby, the timing, mechanisms, and stimulation for aging varies across tissues, depending on the tissue-specific function (Gensler & Bernstein, 1981; Yureneva et al., 2021).

Dystocia is one of the most prevalent and clinically difficult conditions in mouse colonies (Burkholder et al., 2012). This condition can be triggered by multiple factors. For example, stress exposure can disrupt the delivery in humans, pigs, and rodents (Douglas et al., 2002); nutritional imbalance like hypocalcemia or vitamin E deficiency is associated with dystocia in buffaloes, goats, dogs and cats (Sathya et al., 2007; Pretzer, 2008; Bayoumi et al., 2021); and advanced maternal age as a common cause for difficult labor in mice (Wilkinson et al., 2020). In mice, the onset of parturition is determined by progesterone withdrawal associated with a uterine increase in prostaglandin F2alpha (Figure 1) and subsequent ovarian luteolysis. The parturition is thus triggered by a dialogue between the uterus and the ovary. In old mice, progesterone withdrawal is delayed or absent, leading to impaired parturition (Patel et al., 2017). The difference in progesterone decrease between young and old mice likely indicates a disruption in the luteolysis pathway in old mice (Patel et al., 2017). As luteolysis is initiated by prostaglandin F2alpha, it is likely that the alterations in this inductive process precipitate the observed phenotype. The requirement of prostaglandin receptors for progesterone withdrawal and parturition was demonstrated in an experimental knock out of the prostaglandin F2alpha receptor gene (Sugimoto et al., 1997), which mimics the phenotype observed in the aged mice.

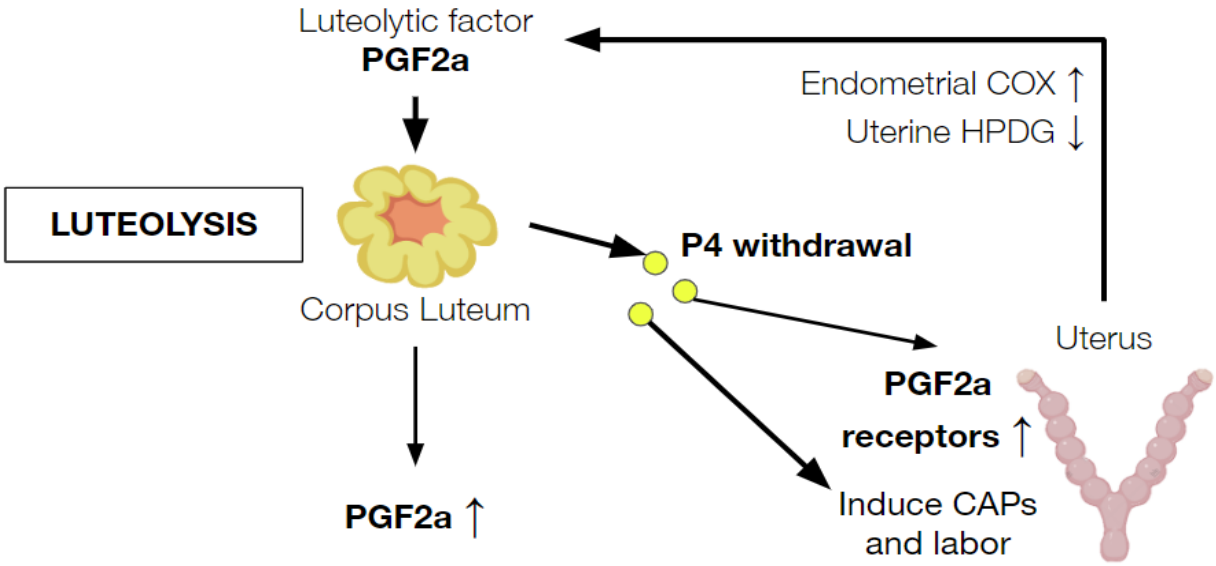

Figure 1 - A diagram illustrating the underlying hormonal mechanisms that lead to parturition in mice. Legend: COX - cyclooxygenase; HPDG - 15-hydroxyprostaglandin dehydrogenase; PGF2a - prostaglandin F2**α**; P4 - progesterone; CAPs - contraction-associated proteins. Based on the work of Ratajczak & Muglia, 2008; and Bezold et al., 2013.
Image source: biorender.com

To understand the complex causality of this phenotype, it is important to understand changes in the ovary as well as the uterus (including the cervix). In this work, we focus on senescence in the uterine and cervical tissues. Upstream (prostaglandin) and downstream (uterine activation and contractility) changes in the aging uterus may contribute to increased gestational length (Yomogita et al. 2022, Herington et al. 2018). Aging has been shown to influence the timing of parturition through abnormal timing of cervical ripening or impaired prostaglandin responsiveness (Patel et al., 2017, Yomogita et al. 2022). In this study, we will conduct an in-depth transcriptional and histological investigation of the mechanisms through which uterine and cervical changes in older mice contribute to the effects of aging on the timing of parturition.

4. Materials and Methods

4.1. Experimental design

In order to unravel the age-related changes in the uterus that may influence gestational length, we compare two age-groups of mice at two time points of pregnancy. The age-groups consist of 6 three months old (henceforth: young) mice at the beginning of their reproductive maturity; and 6 eight months old (henceforth: old) mice at the presumable beginning of the decline of their reproductive function (see Figure 2 for study design). The pregnancy time points were chosen based on the reported dynamics of the serum progesterone levels, where the onset of progesterone withdrawal is at 15.5 dpc (days post copulation), and by 17.5 dpc the levels of progesterone are significantly decreased in the serum of pregnant mice (Holinka et al., 1978; Holinka et al., 1979). Three individuals of each age group were analyzed at each of the two time points. From each mouse tissues were harvested for transcriptomic analysis (endometrium/decidua), for histology (uterus with placenta and uterine cervix) and for hormone measurement (progesterone in blood serum and prostaglandin in uterine tissue). Thus, the same individuals are represented in each kind of data.

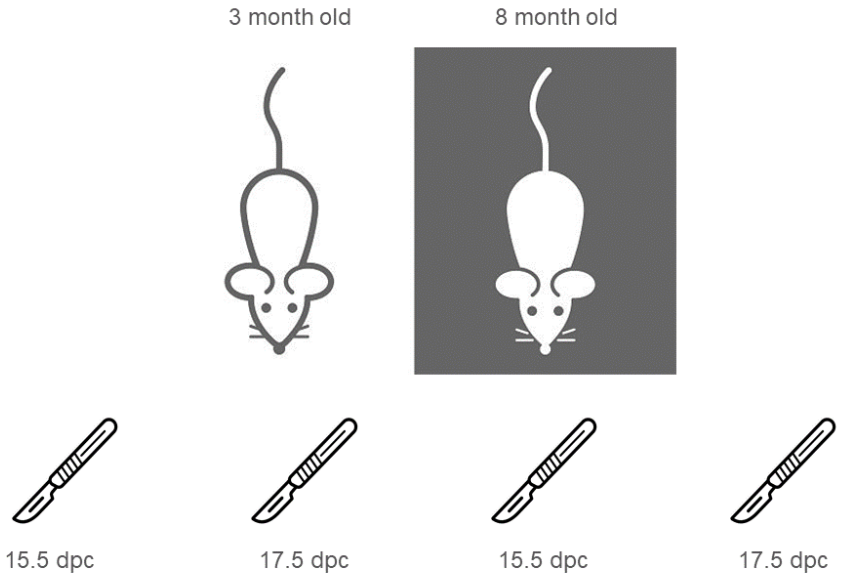

Figure 2 - Experimental design illustrating the age groups of mice we used in our study (young or 3 months old, and old or 8 months old) and the time points we harvested the tissues labeled as dpc - days post copulation.
Image source: biorender.com; istockphoto.com

4.2. Animal husbandry

We used mice from the strain C57 BL/6 (Charles Rivers Laboratories). The mice were housed in an animal facility in accordance with the regulations on animal welfare and ethics of the University of Vienna, under conditions of a 12:12 hour light : dark cycle with a room temperature of 22-24℃. Ad libitum access to food and water with 1,5ml 1%HCl / liter was always secured. After colony mating, mice were weaned from the mother at three weeks of age, in separate cages based on their sex. Female mice were kept in cages together prior to mating (2-4 mice per cage), while males had separated cages if previously mated. Males of all ages (3 months old to 12 months old) were used for matings. The mating was carried out by transferring females in estrus (for staging the cycle see below) into the male cage overnight, and confirming copulation by checking for a vaginal plug the following morning. The noon of the day finding a copulatory plug marks the 0.5 day post copulation (i.e., 0.5 dpc), of the potential pregnancy that lasts approx.19 days in this strain.

4.3. Tissue collection

Animals were euthanized by cervical dislocation. Reproductive tissues (uterine horns and cervix) and blood samples were harvested immediately after euthanasia from 12 mice: 6 young, and 6 old mice (in each age cohort 3 at 15.5 dpc and 3 at 17.5 dpc). First, blood samples were collected with a 1 ml syringe and a needle directly from the heart. Next, the gastrointestinal tract was removed for a better view of the internal organs. The fat, blood vessels and connective tissue, were carefully trimmed from the uterus upon which the pregnant uterus was detached from the body and transferred to a petri dish filled with 1x phosphate-buffered saline (PBS) for dissection under the dissecting microscope. Microdissection of the uterus involved isolation of the cervix for histology, and isolation of segments of pregnant uterus containing single embryos, which was subsequently cut longitudinally at the antimesometrial side opposite of the placenta in order to remove the embryo, while keeping the placenta and/or the placenta-maternal interface intact. The last step was repeated for all of the embryos and corresponding uterine portions in order to acquire tissues for the following procedures: 1) for histology - tissues were stored in a 15 ml tube filled with 4% PFA overnight on a rocker; 2) for RNA sequencing - tissues were stored in 2 ml tubes filled with RNALater solution; and 3) for PGF2a measurement - tissues were flash frozen in liquid nitrogen at dissection in 2 ml cryotubes, and transferred to -80C storage until further analysis.

4.4. Serum preparation

After collection in a 1.5 ml eppendorf tube, the blood sample was sitting at room temperature for 20 minutes. Then it was spun in the centrifuge at 3400 rpm for 30 minutes.

The supernatant (serum) was collected with a micropipette and stored in a new 1.5 ml labeled eppendorf tube at -80℃.

4.5. Tissue processing for histology

In order to stop the decomposition processes, the tissues collected for histology were immediately fixed in 4%PFA on a rocker overnight, so denaturation and coagulation of proteins in the tissues can occur. After fixation, the tissues are soft and thus for good sectioning and staining results, the tissues were treated with a dehydrating agent. For paraffin embedding, dehydration is an important step, as paraffin is a hydrophobic substance and does not penetrate wet tissue effectively. Because of this, water in the tissue should be removed before embedding, which we achieved with a series of graded concentrations of ethanol: 30%, 50% and 70%. This technique prevents mechanical damage to the intracellular structures, which might occur due to the rapid extraction of water from the cells to the dehydrating medium (i.e. ethanol of high concentration). Once the tissues are in 70% ethanol, they can be stored in the fridge at 4℃, or embedded in paraffin. In order to proceed all water must be extracted from the tissues, so higher concentrations of ethanol were used: 95% and two rounds of absolute ethanol. Next, the ethanol is removed by replacement with a cleaning agent/solvent (benzol). At last, melted paraffin was used to penetrate the tissue and replace the solvent. Paraffin blocks were molded in plastic embedding molds and attached to disposable plastic cassettes. Sections were made with motorized, programmable rotary microtome Leica RM2265 with a thickness of 5μm.
Sections from the uterus and the cervix were stained with 4 different techniques: Hematoxylin and Eosin (H&E) – staining the nuclei of the cells purple with hematoxylin, and the cytoplasm and extracellular matrix pink with eosin; for qualitative analysis of all the tissues; Masson's Trichrome - staining the collagen fibers for estimating tissue remodeling and/or fibrosis in particular in cervix; and Periodic Acid-Schiff (PAS) Stain - evaluating the amount of carbohydrates in general and glycogen specifically, in the uterine tissue. The protocol for the PAS staining was modified with a step that included amylase treatment and distilled water treatment at the temperature of 37℃ of neighborhood slides from the same individuals.

4.6. Image analysis

Where relevant, the stained histological sections were subjected to imaging and image analysis with the EVOS M7000 Imaging System (ThermoFischer). The thickness of columnar epithelium in the Masson’s Trichrome-stained sections was measured with the line tool from the EVOS Analysis Software, whereas the statistical calculations on these measurements were performed in MS Excel. The intensity of staining in PAS stained sections was quantified with Celleste 6 Image Analysis Software using the following var-

iables: Intensity Uncalibrated (lum) - average uncalibrated luminance (intensity or optical Density) of region; Intensity Red (lum) – region's red mean value; and YIQ color Q (lum) - Q component (chrominance information) of YIQ color space, chrominance in purple-green range. The statistical analysis on the results from these measurements was performed in MS Excel.

4.7. Hormone assays

Concentration of progesterone in blood serum was measured with a competitive enzyme-linked immunosorbent assay (ELISA), using the Mouse Progesterone ELISA kit (Crystal Chem). We used 10 µl of serum from each replicate, with 50 µl incubation buffer and 50 µl conjugation solution (horseradish peroxidase) in a 96-well microplate with progesterone antiserum-coated wells. Optical density of each replicate and standard was measured with an absorbance reader (SpectraMax ABS by Molecular Devices) at 450/630 nm wavelength, using (SoftMax Pro 7.1 software). The results from the optical density measurement are inversely proportional to the concentration of progesterone.

Prostaglandin F2α measurements were conducted on flash frozen uterine tissue samples. The weighed tissues were first homogenized in flash freezing tubes containing 70% ethanol and a stainless-steel bead, using a tissue lyser (Precellys Evolution). Next, ethanol was removed using nitrogen gas in an evaporator, to prepare the sample to be measured using competitive ELISA Mouse PGF2α kit (antibodies.com). Samples diluted in a buffer (Sample Dilution Buffer) were loaded into PGF2α-precoated wells along with standards and Anti-PGF2a Antibody (Biotin) in a 96-well microplate. HRP-conjugated streptavidin was used to catalyze the later added TMB substrate, which results in blue coloration. Stop Solution was used to terminate the reaction, which changed the color from blue to yellow. The intensity of the signal was measured with an absorbance reader (SpectraMax ABS) at 45 nm, using SoftMax Pro 7.1 software. The concentration of PGF2α is inversely proportional to the intensity of the measured signal.

4.8. RNA extraction

After dissection, uterine tissue was stored in RNALater Solution (Invitrogen) at -20℃. Prior to RNA extraction, the uterine tissue was micro-dissected and half of the endometrium was homogenized in a lysis buffer with dithiothreitol (DTT), using tissue lyser (Precellys Evolution) in flash freezing tubes containing a stainless-steel bead. RNA extraction with RNEasy mini kit (Qiagen) was performed according to the manufacturer's protocol. Isolated RNA was eluted in 45 ml sterile water. DNA was removed from the samples using Turbo DNA-free kit (Invitrogen) Protocol.

4.9. Acquiring and analysis of transcriptomic data

Library prep and sequencing was performed by NovoGene with Illumina, providing pair-end reads of 150 base pairs. The samples had RNA concentrations in the range of 73.1-107.8 ng/ml and all passed RNA quality control prior to sequencing (Bioanalyzer).

All analyses of transcriptomic data were performed using R, the Project for Statistical computing (https://www.r-project.org; Version 4.3.1). Quality control of the raw reads from the sequencing was performed by multiQC. Each individual read was mapped to a mouse genome (GRCm38.p6) from Ensembl with STAR, using The Life Science Compute Cluster (LiSC) at the University of Vienna. Primary assembly was stored in BAM file format, quantified by Gene Counts with sequences containing one less base pair than the output of the sequencing.
All files were loaded and merged in a list in RStudio. Differential gene expression analysis based on the negative binomial distribution was performed using the DESeq2 package (Love at al., 2014) from Bioconductor (http://www.bioconductor.org). Variance-stabilized transformed data (vst function from DESeq2 package) resulting from the differential gene expression analysis were used to arrive at the relationships among samples using principal component analysis (PCA) and correlation. Next, integrated analysis of factors by employing the DESeq2 package was performed. Log2 fold change values were shrunken with lfcShrink function. The similarity between samples was visualized by transforming the measurements onto log ratio (M) and mean average (A) scales, which were then plotted in MA plots. We performed separate analysis of time points within age groups in order to look at differential expression with combined factors (young 15.5 dpc vs. young 17.5 dpc and old 15.5 dpc vs. old 17.5 dpc). The correlation of log2 fold change between time points and PCA loading values were plotted. This was followed by a functional analysis of differentially expressed genes using enrichGO for Gene Ontology (Thomas et al., 2022) and Fast Gene Set Enrichment Analysis (fgsea, Mootha et al., 2003; Subramanian et al., 2005). Genes of interest (genes with contrasting patterns of expression) were plotted so we can see how they change differently. All plots were produced with ggplot from ggplot2 package.

4.10. Statistical Analysis

Data visualization and statistical calculations (T-test for independent samples, 2-tailed) for progesterone and PGF2α results, as well as for the colorimetry and histological measurements were performed using MS Excel.

5. Results

5.1. Hormone measurements

The results of the progesterone analysis are plotted in Figure 3a. Statistical analysis (2-tailed T-test for independent samples) was performed between groups: young 15.5 dpc vs. young 17.5 dpc (p=0.2); old 15.5 dpc vs. old 17.5 dpc (p=0.5); young 15.5 dpc vs. old 15.5 dpc (p=0.8); young 15.5 dpc vs. old 15.5 dpc (p=0.9). These results imply that there are no significant differences between the samples, neither due to the pregnancy stage, nor due to the age.

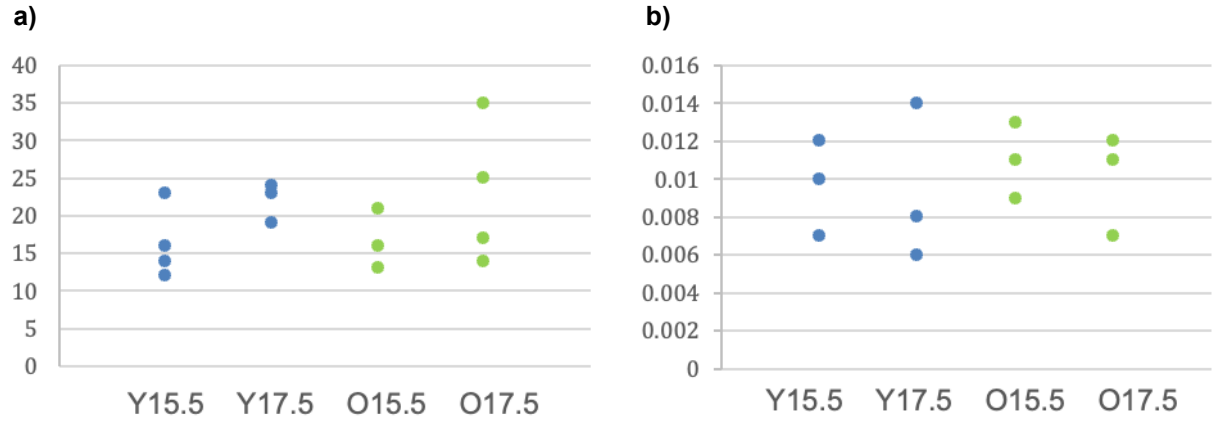

Figure 3 – a) Progesterone levels in old mice (blue) and young mice (green), at 15.5dpc (Y15.5 and O15.5) and 17.5dpc (Y17.5 and O17.5). On the X-axis age groups at early and late time points are plotted, and on the Y-axis the average concentration of progesterone in ng/ml. Young mice at 15.5 dpc and old mice at 17.5 dpc have 4 replicates each, as opposed to the other groups who have 3 replicates each. b) Prostaglandin F2α (PGF2α) levels in young (blue) and in old mice (green), at 15.5dpc and 17.5dpc. On the X-axis age groups at early and late time points are plotted, and on the Y-axis the average concentration of PGF2α in pg/ml.

Results from the PGF2α analysis (Figure 3b) are revealing average concentration for young mice of 0.0065 pg/ml at 15.5dpc and 0.00883 pg/ml at 17.5dpc; and for old mice, 0.011 pg/ml at 15.5dpc, and 0.001 pg/ml at 17.5dpc (Fig4). T-test reveals no significant difference between the samples: young 15.5 dpc vs. young 17.5 dpc (p=0.9); old 15.5 dpc vs. old 17.5 dpc (p=0.6); young 15.5 dpc vs. old 15.5 dpc (p=0.5); young 15.5 dpc vs. old 15.5 dpc (p=0.8).

All together, we did not detect significant differences in measured hormonal levels in our samples, either between the stages within age groups, nor between the age groups.

5.2. General structure of utero-placental units and cervices does not differ between age groups

To understand the structural changes during pregnancy and aging, histological sections of pregnant uteri and cervices from young and old mice at the two time points were stained with Hematoxylin and Eosin (Figure 4 and Figure 5). Tissues from the uterine sections contain myometrium (M), maternal decidua (D), placental junctional zone (JZ), placental labyrinth (L) and yolk sac (YS) – the latter is absent from the section of young uterus at 17.5 dpc. In all samples, the placenta makes up the largest part of the tissue. Images in figure 5 a) through c), show the normal changes in the young uterus during pregnancy, while d) through g), show the changes in the old mice during pregnancy. The decidua is not a prominent structure in both age groups, and appears almost absent at later time points. The blood vessels in the labyrinth and the junctional zone become more prominent at 17.5 dpc compared to 15.5 dpc in young mice. The junctional zone contains large quantities of glycogen-containing trophoblast cells (GC) (see supporting evidence by Schiff staining) and spongiotrophoblast cells. There appears to be no obvious difference in tissue structure of the utero-placental samples between age groups nor time points. H&E stained section from the cervical tissue shows two general compartments: stroma (composed by fibrous connective tissue) and luminal epithelium. The epithelium consists of a single layer of mucin-secreting columnar cells, and is located on the endocervical lumen and the endocervical glands. The columnar epithelium (labeled CE-EC in Figure 5) is more pronounced at 17.5 dpc in both age groups (averages across 4 animals: young mice 50.22 μm; old mice 32.95 μm), as opposed to 15.5 dpc (young mice 29 μm; old mice 27.21 μm). The squamous epithelium of the ectocervix (labeled SE-EC in Figure 5) is more pronounced at 17.5 dpc in young mice (averages across 4 animals: young mice at 15.5 dpc 30.42 μm; and 17.5 dpc 48.91 μm), and displays the opposite pattern in old mice (old mice at 15.5 dpc 36.84 μm; and 17.5 dpc 42.31 μm).

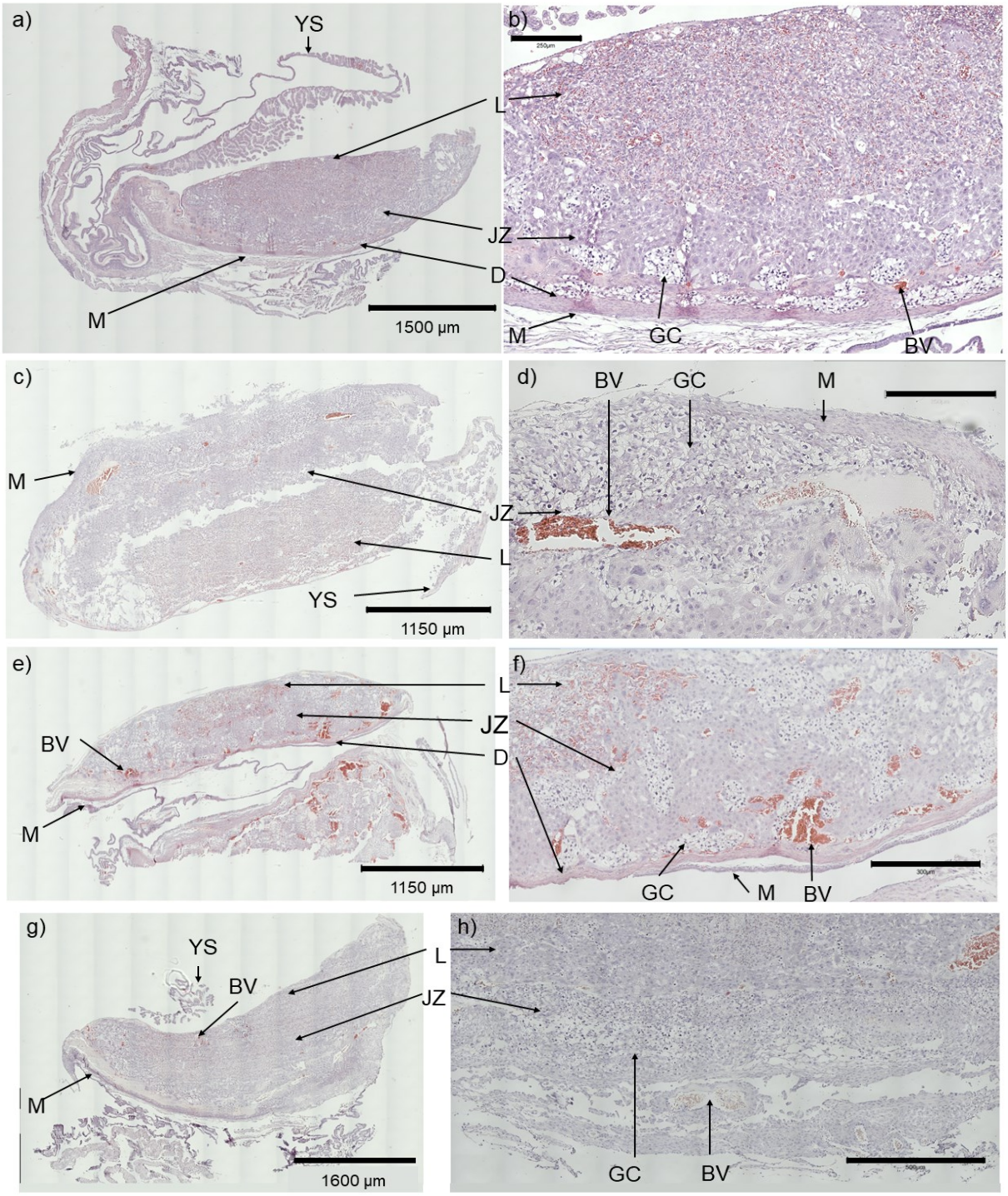

Figure 4 - Hematoxylin and Eosin-stained 5 µm thick transversal sections of uterine and placental tissues of: a) a young mouse at 15.5 dpc (magnification 20x, scale bar 1500 µm); b) a young mouse at 15.5 dpc (40x, scale bar 250 µm); c) a young mouse at 17.5 dpc (20x, scale bar 1150 µm); d) a young mouse at 17.5 dpc (40x, scale bar 250 µm); e) an old mouse at 15.5 dpc (20x, scale bar 1150 µm); f) an old mouse at 15.5 dpc (40x, scale bar 300 µm); g) an old mouse at 17.5 dpc (20x, scale bar 1600 µm); h) an old mouse at 17.5 dpc (40x, scale bar 500 µm). In all sections, the placenta makes up the largest portion of the tissues. The following structures are labeled with their respective acronyms: myometrium (M), decidua (D), junctional zone (JZ), labyrinth (L), yolk sac (YS), glycogen cells (GC), and blood vessels (BV). Blood vessels are more visible in the labyrinth and the junction zone at 17.5 dpc compared to 15.5 dpc in young mice, whereas in old mice tissues appear to be more vascularized at 15.5 dpc than at 17.5 dpc.

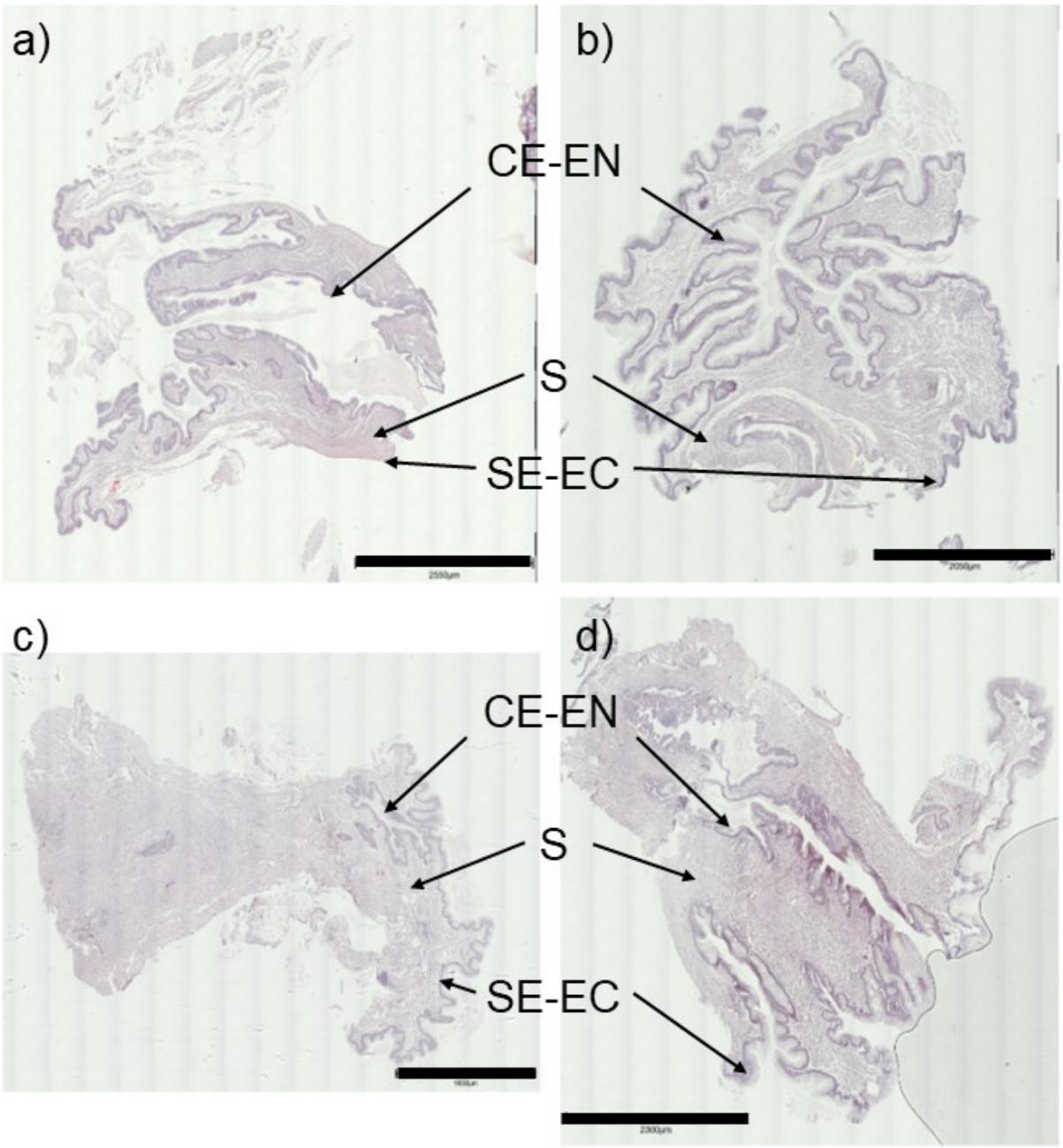

Figure 5 - Hematoxylin and Eosin-stained 5 µm longitudinal sections of cervixes of: a) a young mouse at 15.5 dpc (magnification 20x, scale bar 2550 µm); b) a young mouse at 17.5 dpc (20x, scale bar 2050 µm); c) cervix of an old mouse at 15.5 dpc (20x, scale bar 1850 µm); d) an old mouse at 17.5 dpc (20x, scale bar 2300 µm). The stroma is labeled with an S. Columnar epithelium of the endocervix (CE-EN) is more pronounced at 17.5 dpc, compared to 15.5 dpc in both age groups. Squamous epithelium of the ectocervix (SE-EC), is more pronounced at 17.5 dpc, compared to 15.5 dpc in young mice, and opposite in old mice. The image of the cervix of an old mouse at 17.5 dpc is suboptimal, as the section plane is tilted relative to the cervical canal, on the right side is the proximal (uterine) side of the cervix, and on the left side is the distal (vaginal) side of the cervix.

5.3. Distribution of collagen in the cervix of young and old pregnant mice

To understand whether the reported tendency of older mice for delayed parturition may also be reflected as delayed remodeling of the cervix, we stained the cervix of both age classes using Masson's Trichrome, which stains collagen blue. The red stain in these tissues is denoting cytoplasm, muscle and blood.
As expected, we see strong collagen staining in the cervical stroma. Figure 6 shows a difference in the cervical tissues between age groups, with larger interstitial spaces (white areas) between collagen fibers in young mice, as opposed to old mice. This is especially apparent at 17.5 dpc where the interstitial spaces in old mice are much less abundant.

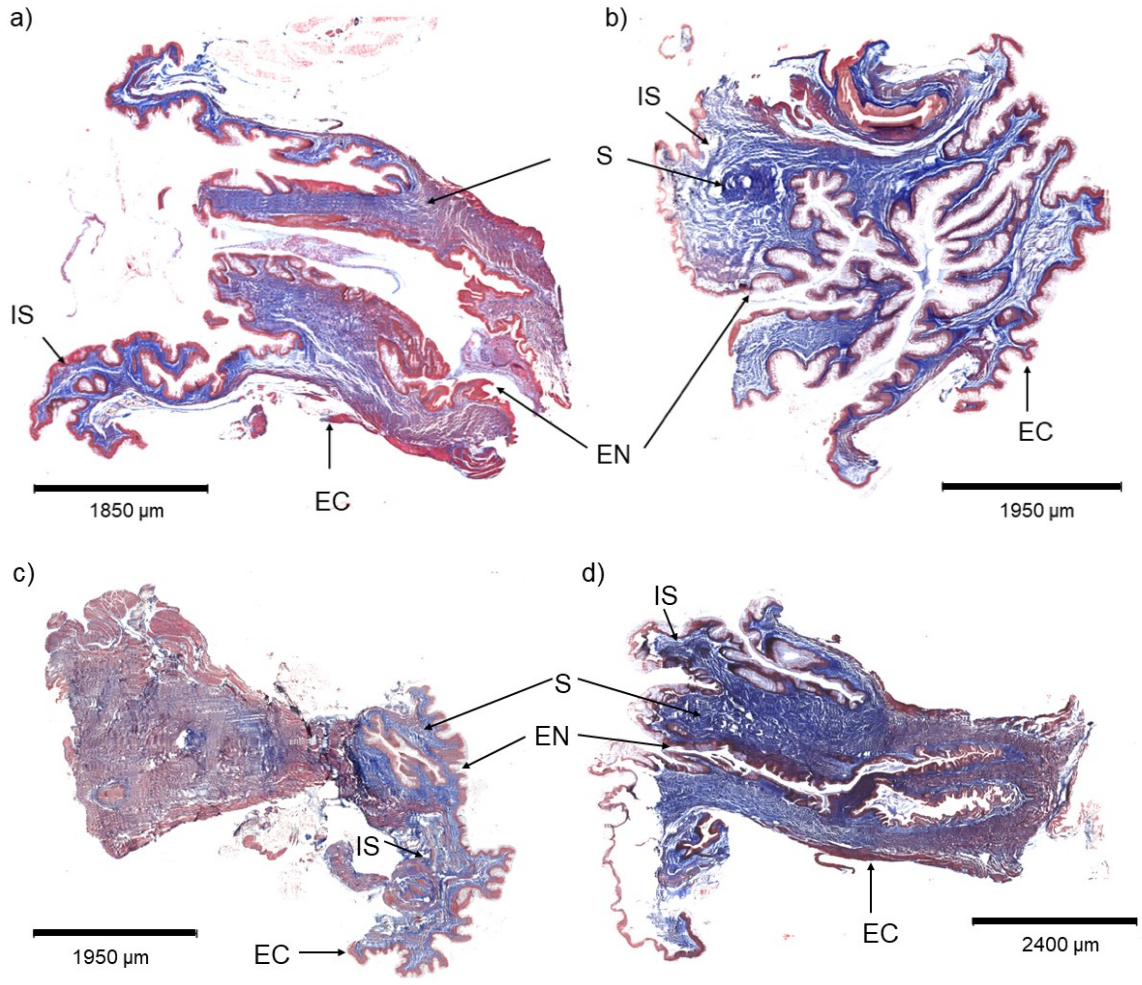

Figure 6 - Masson's Trichrome-stained 5 µm thick longitudinal sections of cervical tissues: a) young mouse at 15.5 dpc; b) young mouse at 17.5 dpc; c) old mouse at 15.5 dpc; d) old mouse at 17.5 dpc. All images are taken with 20x magnification. The following structures are labeled: stroma (S), endocervix (EN), ectocervix (EC), interstitial spaces (IS). Blue stain indicates collagen fiber, while red stain denotes cytoplasm, muscle cells and blood. Young mice display more interstitial spaces (white areas) between collagen fibers as opposed to old mice. The image for the cervix of an old mouse at 17.5 dpc (Fig 7 d) is suboptimal (see the comment in caption of Fig.6).

5.4. Glycogen content of the tissue

Periodic acid–Schiff (PAS) staining with and without amylase treatment was performed on utero-placental tissues to estimate their glycogen content. Periodic-Schiff stain colors the carbohydrates pink, and by pretreatment with amylase, the glycogen portion is degraded, enabling its measurement by comparison. By using this method, we detected glycogen in the uterine-placental unit. In Figure 7, the results from the PAS staining with amylase treatment (left) and distilled water incubation (right) of uterine-placental unit is shown. Uterine tissue is marked with U in the figures, labyrinth with L, and junction zone with JZ. Complementary to the H&E staining, the results from the PAS staining clearly mark the layer of glycogen-containing trophoblast cells in the junctional zone of the placenta (labeled with GC in Figure 7). The glycogen-containing trophoblast cells appear as large, empty cells in a H&E staining (Figure 4), while they gain intense pink coloration in PAS-stained tissues (Figure 7).

Placenta attached to the uterine tissue in young mice at 15.5 dpc contain higher levels of glycogen, while young mice at 17.5 dpc and old mice at both time points contain very low levels of glycogen.

We then assessed the glycogen levels in the labyrinth and the junction zone in these tissues by measurement of intensity of staining. We used 3 different variables available in Celleste 6 image analysis software, capturing somewhat different aspects of intensity of staining, to test for consistency thus providing a robust assessment. These variables are: the Intensity Uncalibrated (lum), Intensity Red (lum), and YIQ color Q (lum). The results shown in Figure 8 are illustrating higher levels of glycogen content in young mice at 15.5 dpc, compared with the other age groups and time points. The statistical significance of these results was confirmed with a T test, where young mice at 15.5 dpc had $p \leq 0.05$ when compared to multiple groups (in the labyrinth: young 15.5 dpc vs. old 15.5 dpc for intensity uncalibrated and intensity red; young 15.5 dpc vs. old 17.5 dpc for intensity uncalibrated, intensity red and YIQ color Q; and in the junction zone: young 15.5 dpc vs. old 15.5 dpc for intensity uncalibrated, intensity red and intensity red and YIQ color Q; young 15.5 dpc vs. old 17.5 dpc for intensity uncalibrated, intensity red and YIQ color Q).

The results using measures of different aspects of color intensity are consistent (Figure 8).

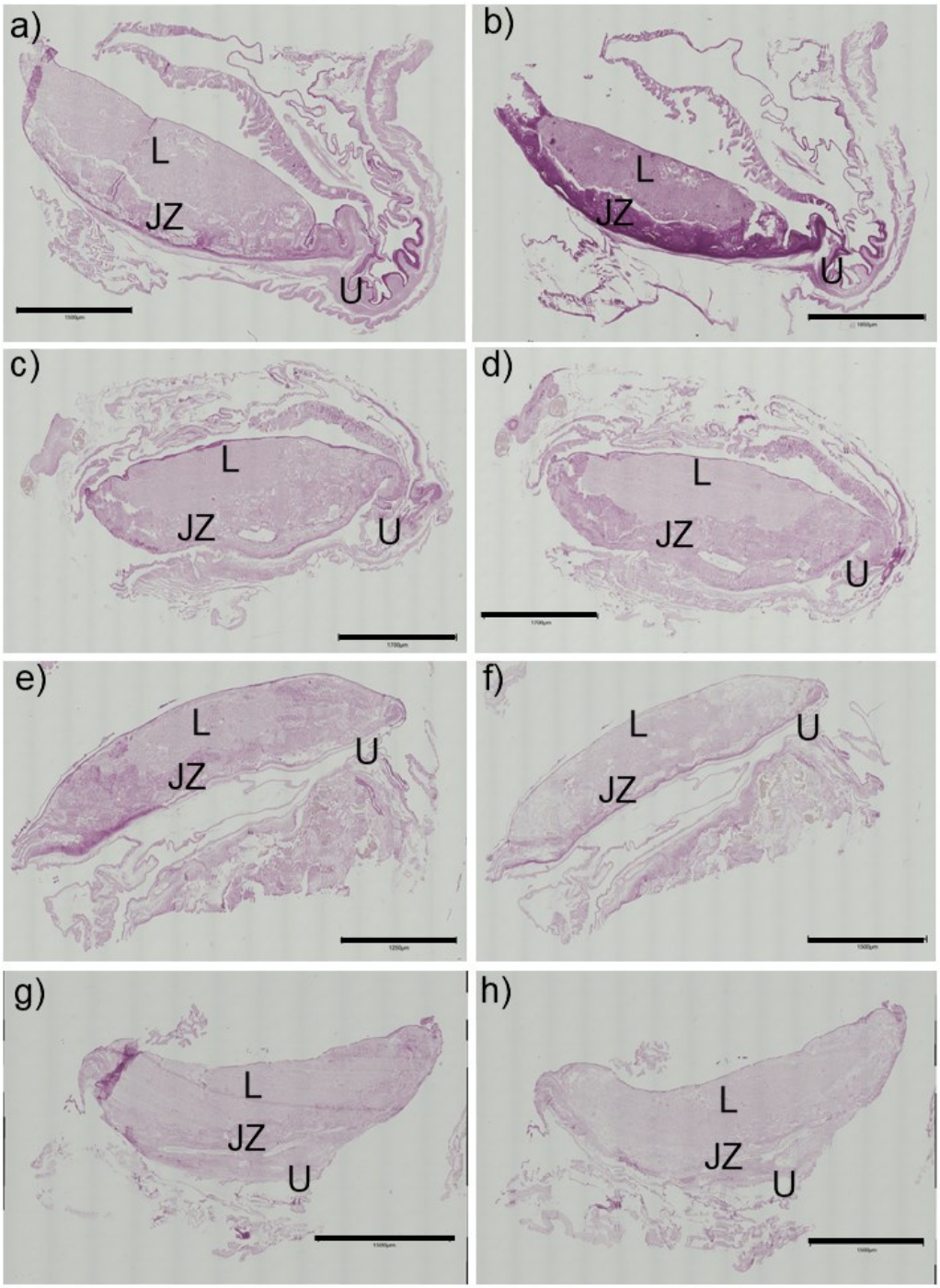

Figure 7 - Periodic acid–Schiff stain staining of uterine and placental tissues: a) of a young mouse at 15.5 dpc treated with amylase (20x, scale bar 1500 µm); b) of a young mouse at 15.5 dpc treated with distilled water (20x, scale bar 1850 µm); c) of a young mouse at 17.5 dpc treated with amylase (20x, scale bar 1700 µm); d) of a young mouse at 17.5 dpc treated with distilled water (20x, scale bar 1700 µm); e) of an old mouse at 15.5 dpc treated with amylase (20x, scale bar 1250 µm); f) of an old mouse at 15.5 dpc treated with distilled water (20x, scale bar 1500 µm); g) of an old mouse at 17.5 dpc treated with amylase (20x, scale bar 1500 µm); h) of an old mouse at 17.5 dpc treated with distilled water (20x, scale bar 1500 µm). The sections treated with amylase (left side) are visibly lighter than sections treated with distilled water. The following structures are labeled in the images: labyrinth (L), junctional zone (JZ) and uterine tissues (U).

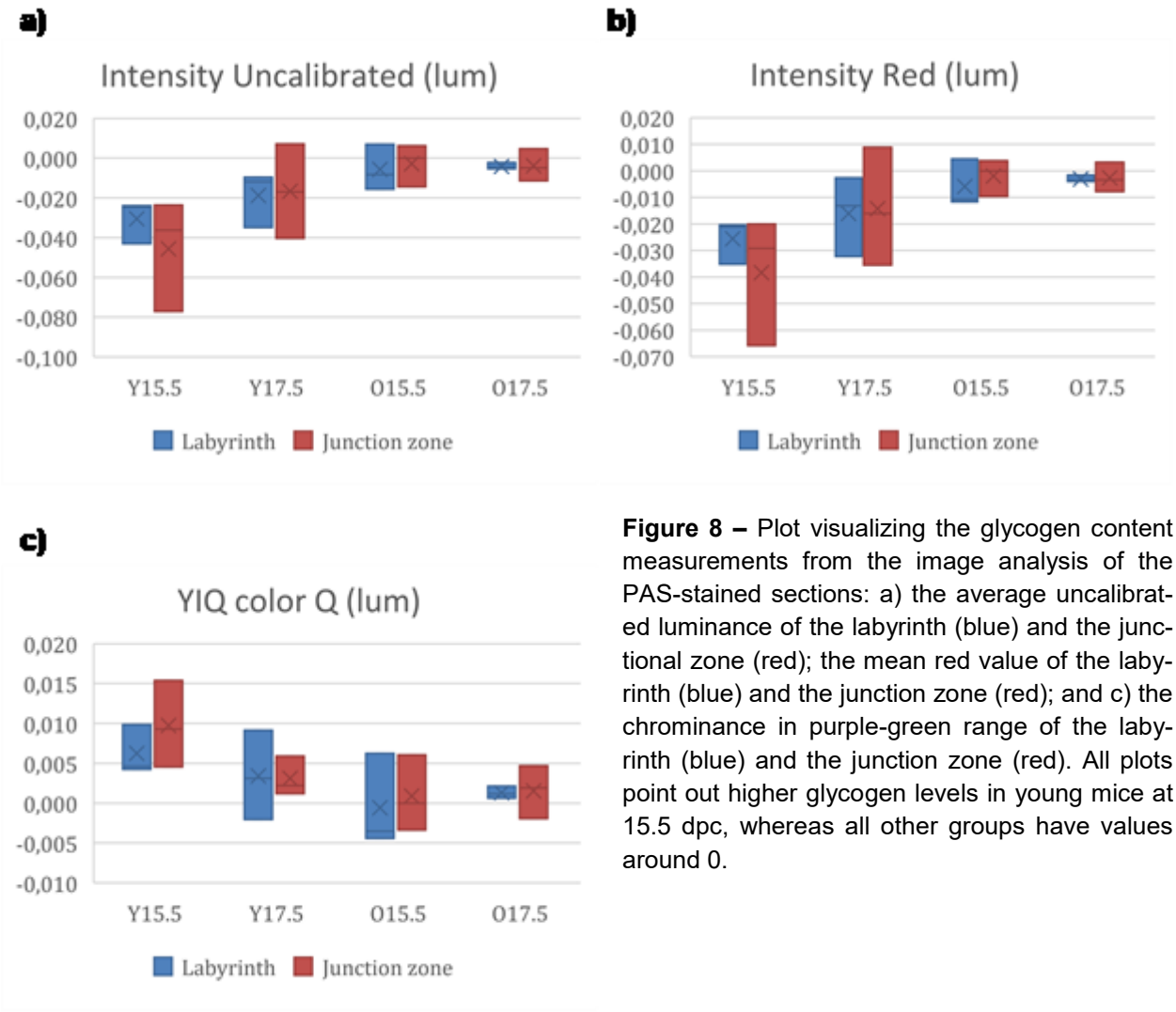

Figure 8 – Plot visualizing the glycogen content measurements from the image analysis of the PAS-stained sections: a) the average uncalibrated luminance of the labyrinth (blue) and the junctional zone (red); the mean red value of the labyrinth (blue) and the junction zone (red); and c) the chrominance in purple-green range of the labyrinth (blue) and the junction zone (red). All plots point out higher glycogen levels in young mice at 15.5 dpc, whereas all other groups have values around 0.

5.5 Transcriptome analysis reveals effects of aging on gene expression

Results from the MultiQC analysis show that the number of aligned reads in the transcriptome of young mice at 15.5 dpc ranges from 20.4M to 24.2M, and for young mice at 17.5 dpc from 19.5M to 25.5M. The numbers for old mice range from 20.4M to 22.1M at 15.5 dpc, and 17.7M to 25.1M at 17.5 dpc. Number of reads for gene counts ranges between 17 471 643M and 20 816 893M for young mice at 15.5 dpc, 15 939 558M and 21 976 282M for young mice at 17.5 dpc, 17 612 753M and 18 946 856M for old mice at 15.5 dpc, and 14 951 492M and 21 496 842M for old mice at 17.5 dpc. Initial data analysis in RStudio reveals 53 801 expressed genes in the decidua of all replicates at a level of transcription. After filtering (>= 10), 19 483 genes remained that we considered expressed. Un-normalized counts were used for analysis with DeSeq2, whose output was used to look at relationships among samples. General relationships among transcriptomes of the samples were examined by using the principal component analysis (PCA). Figure 9 shows the first two principal components together explaining 68,9% of

the variation between samples. The first principal component (43,8% of variation) separates young mice at the later pregnancy from young and old mice at the earlier pregnancy and old mice at the later pregnancy, suggesting that the old mice did not transition into the transcriptome characteristic of later pregnancy. The second principal component (25,1% of variation) captures the difference between the two stages of pregnancy in old mice. These results suggest that the two age groups cluster together in the early pregnancy, but change differently across time points, the change in young mice being captured by the PC1 and the change in the old mice by the PC2. Because the results from the PCA are highlighting differences in expression between young and old mice at 17.5 dpc, we further examine genes that exhibit differences in their dynamics of expression between age groups.

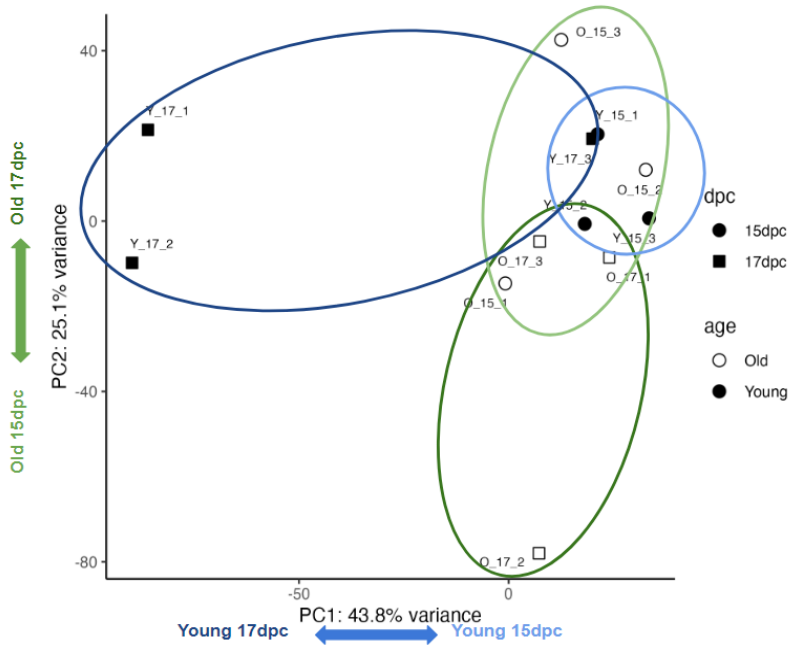

Figure 9 - PCA plot. Major axis of variation corresponds to differences between times for young (PC1) and differences between times for old (PC2).

MA plots shown in Figures 10 and 11 display the change in expression for each gene at two time points of gestation (15.5 dpc and 17.5 dpc), plotted against its mean expression across all samples in young mice (Figure 10) and in old mice (Figure 11). This allows us to look at the increase and decrease of expression in one age group across time points. When we compare the MA plots in Figure 10 and Figure 11, we can clearly notice the higher number of genes that increase in expression in young mice from 15.5 dpc to 17.5 dpc, as opposed to old mice. The decrease of expression from 15.5 dpc to 17.5 dpc is similar between age groups. The higher number of genes changing expression in young mice is illustrated also with Euler plots in Figure 9. The increase of expression refers to genes upregulated at 17.5 dpc, a time point where 839 genes were found in young mice and 42 in old mice, with a small overlap between age groups. The decrease of expression is referring to genes upregulated at 15.5 dpc relative to 17.5 dpc where 141 genes were found in young and 149 genes in old mice.

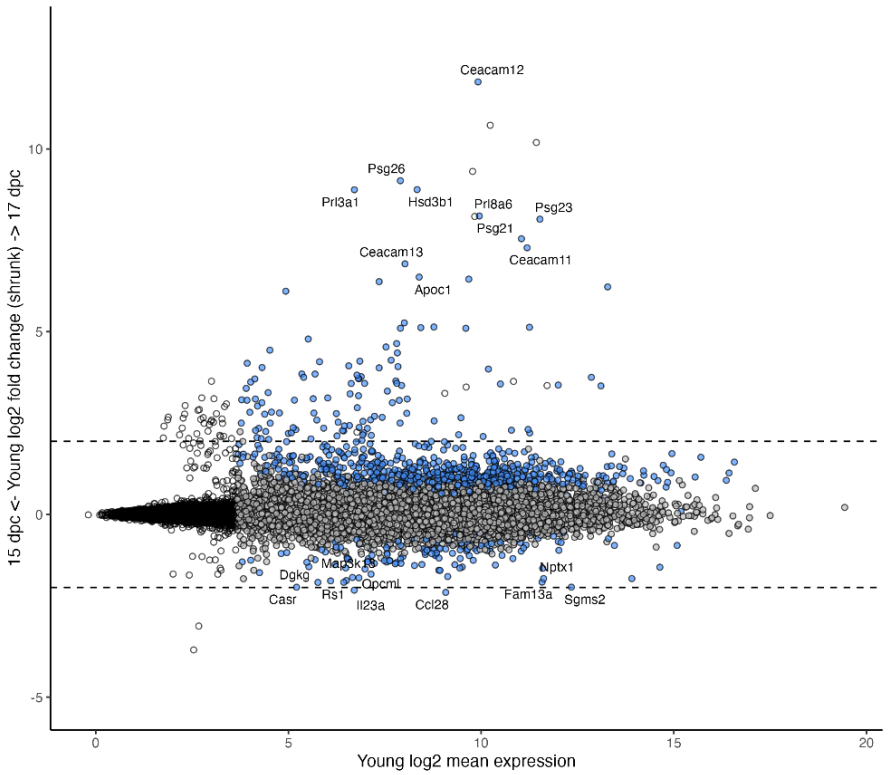

Figure 10 - MA plot displaying the log2 fold change compared with mean expression of genes in young mice. Each data point represents a gene, with statistical significance labeled in blue. Points that fall above the positive threshold on the y-axis indicate upregulated genes at 17.5 dpc, while points that fall below the negative threshold on the y-axis indicate downregulated genes at 17.5 dpc.

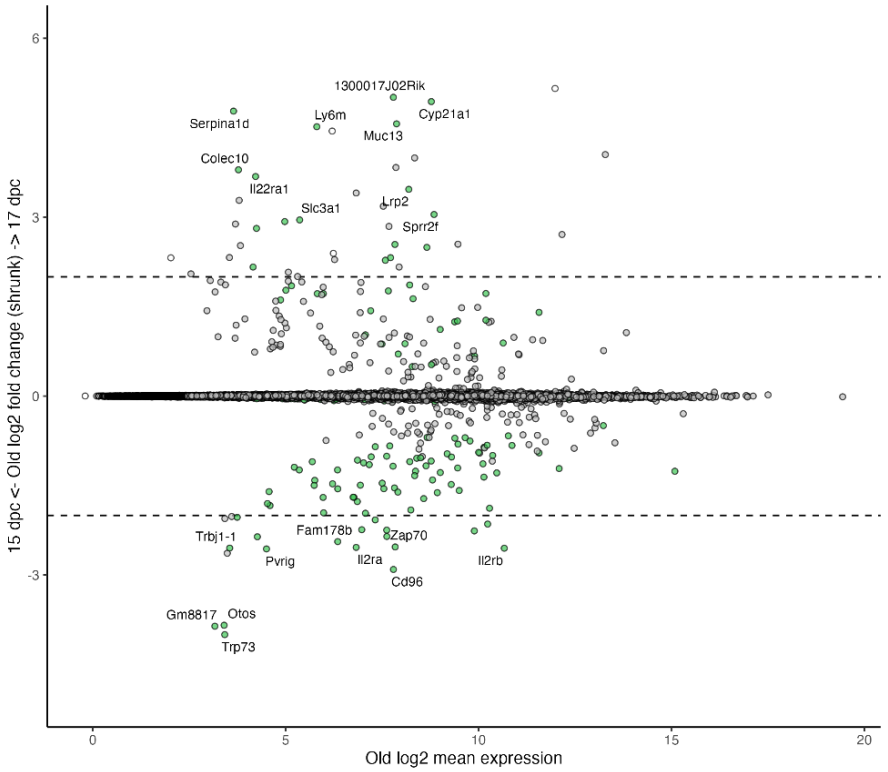

Figure 11 - MA plot displaying the log2 fold change compared with mean expression of genes in old mice. Each data point represents a gene, with statistical significance labeled in green. Points that fall above the positive threshold on the y-axis indicate upregulated genes at 17.5 dpc, while points that fall below the negative threshold on the y-axis indicate downregulated genes at 17.5 dpc.
In comparison with the data from young mice (Figure 10), old mice exhibit lower number of upregulated and downregulated genes.

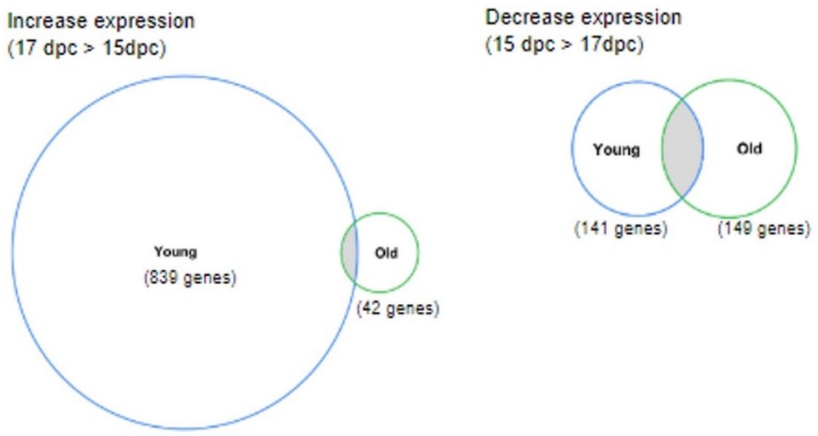

Figure 12 - Euler plots showing the overlap between age groups and highlighting the much larger set of genes with pregnancy stage-related gene expression increase in young compared with old mice.

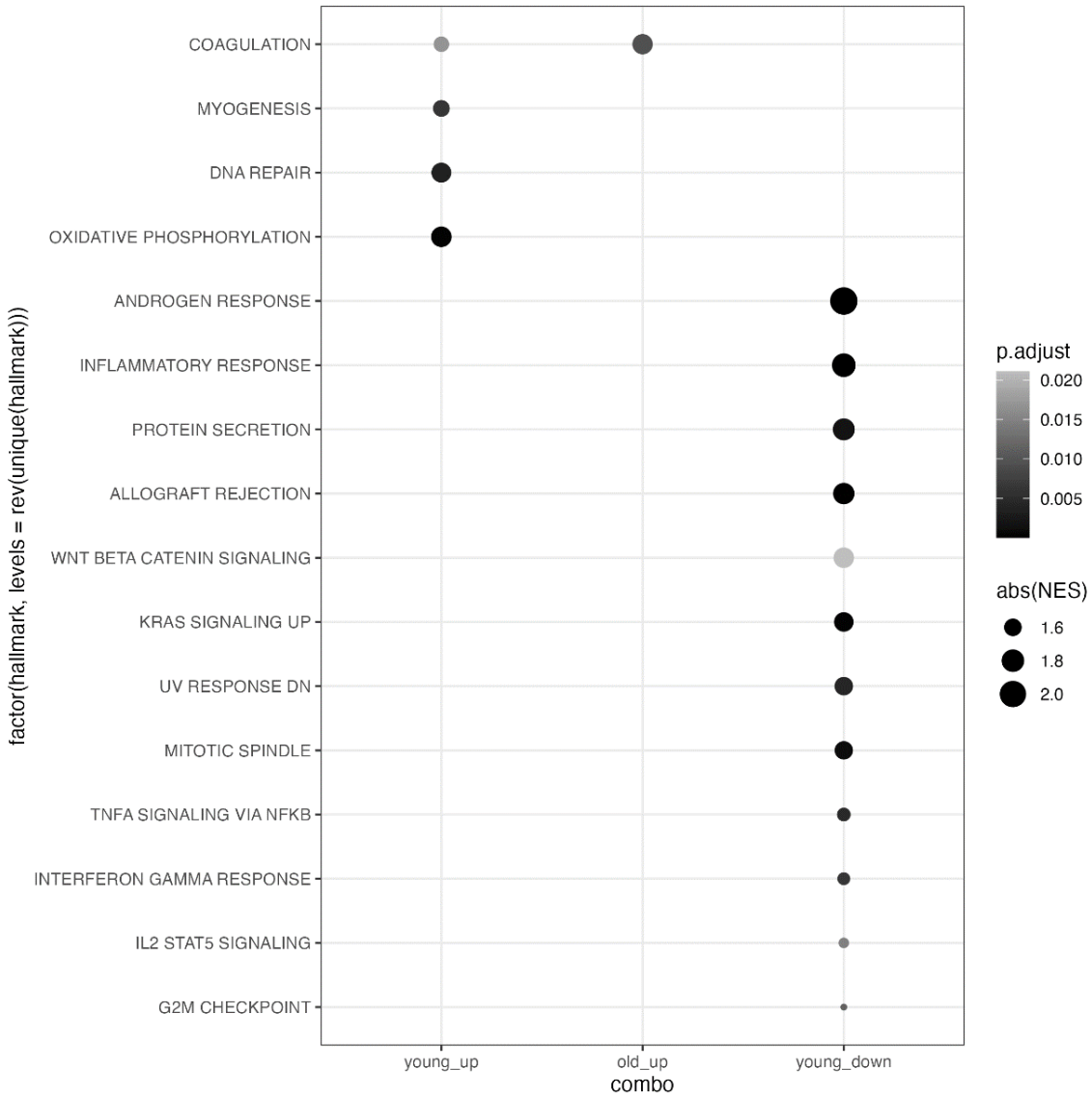

Figure 13 - Gene set enrichment, overlap in coagulation between young and old up. Extensive enrichment for young down but not old.

We next consider the genes differentially expressed between the early and late timepoints in young and old mice separately and their potential functional importance. In young mice, Gene Set Enrichment Analysis (GSEA - Mootha et al., 2003; Subramanian et al., 2005) highlights upregulated genes associated with 4 hallmarks, and downregulated genes associated with 12 hallmarks from 15.5dpc to 17.5dpc (Table 1). In old mice, only a single hallmark (HALLMARK_COAGULATION) was detected among genes significantly upregulated from 15.5dpc to 17.5dpc. There is an overlap between the genes Apoa1 and Mmp10 (in association with the HALLMARK_COAGULATION) between age groups, which suggests that some aspect of coagulation is upregulated from 15.5dpc to 17.5dpc in both age groups. There is an extensive enrichment for downregulated genes in young mice (see Table 1), and none for old mice.

HALLMARK	Age	Change	Genes
COAGULATION	young	up	Apoc1/Apoa1/Fgg/Trf/Mmp15/S100a13/Csrp1/Mmp11/Hmgcs2/Ang/Gnb2/Mmp10/Klk8/Iscu/Crip2/Maff/Proc/S100a1/Comp/Htra1/Bmp1/Pros1/Mmp7/Rapgef3/C1qa/Msrb2
MYOGENESIS	young	up	Kcnh1/Foxo4/Fxyd1/Tnnt1/Tpm2/Bdkrb2/Des/Ptgis/Ckb/Tnnc1/Myl4/Smtn/Eno3/Pdlim7/Gadd45b/Tagln/Bin1/Sh3bgr/Mapk12/Lsp1/Hdac5/Cryab/Sod3/Ckm/Bag1/Rit1/Acta1/Ncam1/Dmpk/Actn3/Tnnt3/Kcnh2/Itgb5/Cav3/Myl6b/Fabp3/Ak1/Crat/Psen2/Pfkm/Casq2/Tgfb1/Itga7/Speg/Ocel1/Pick1/Cox7a1/Gaa/Plxnb2/Ppp1r3c/Efs/Myl7/Fst/Syngr2
DNA REPAIR	young	up	Ada/Aprt/Cda/Ercc1/Edf1/Bola2/Sac3d1/Nt5c/Zfp707/Gtf2f1/Supt4a/Nelfe/Polr2f/Pold1/Poll/Adrm1/Taf10/Polr2i/Polr2j/Dad1/Pold4/Vps37d/Rfc2/Taf1c/Gpx4/Tarbp2/Nelfcd/Pola2/Vps28/Gtf2h5/Guk1/Snapc4/Taf9/Gtf3c5/Dguok/Snapc5/Dut/Polr2h/Ddb1/Polb/Ercc8/Rbx1/Ak1/Npr2/Impdh2/Tk2/Polr2e/Aaas/Cant1/Ercc2/Polr3c/Ssrp1/Polr2c/Polr1d/Alyref/Mpc2/Polr2d/Brf2/Rad52/Gsdme/Lig1/Nelfb/Rfc4/Supt5/Surf1
OXIDATIVE PHOSPHORYLATION	young	up	Timm13/Uqcr10/Ndufa2/Uqcr11/Atp5e/Ndufs7/Uqcrq/Atp5o/Cox4i1/Ndufb7/Atp5d/Ndufs6/Ldhb/Mrpl11/Atp5j2/Ndufs8/Timm50/Cox6a1/Atp5k/Mrps11/Ndufv1/Ndufs3/Mrpl34/Mrps15/Ndufa5/Etfb/Ndufc1/Mgst3/Acaa2/Cox7a2/Cox6b1/Atp5g1/Polr2f/Cox5b/Ech1/Uqcrc1/Acaa1a/Mrps12/Uqcrh/Atp5h/Gpx4/Cox6c/Ndufa3/Hsd17b10/Cox8a/Ndufs4/Ndufb5/Ndufa8/Got2/Atp6v1f/Ndufa7/Ndufv2/Mdh2/Ndufa4/Mrps30/Tcirg1/Iscu/Bax/Ndufa1/Cyc1/Cyb5r3/Gpi1/Ndufs2/Supv3l1/Slc25a4/Idh3g/Ndufb6/Retsat/Atp5j/Fxn/Hadha/Ndufa6/Ndufb8/Vdac3/Bckdha/Ndufb3/Atp6v0b/Cox7b/Cox7a2l/Bdh2/Sdhb/Cox7c/Grpel1/Surf1/Tomm22/Mrpl15/Timm9/Ndufab1/Atp5g3/Oxa1l/Slc25a3/Idh2/Atp5pb/Decr1
COAGULATION	old	up	Apoa1/F2/Serpina1b/Cfi/Mmp10/Pf4/Thbs1
ANDROGEN RESPONSE	young	down	Klk1b21/Abhd2/Akap12/Ptpn21/Dhcr24/Adamts1/Ncoa4/Sgk1/Lifr/Slc26a2/Hmgcs1/Ccnd1/Tpd52/Slc38a2/Ngly1/Gnai3/Cdc14b/Elovl5/Ptk2b/Itgav/Gpd1l/Zmiz1/Uap1/Arid5b/Rps6ka3/Sec24d/Klk1/Stk39/Pgm3/Gucy1a1/Scd2/Herc3/Lman1/Dnajb9/Cdk6/Sms/Idi1/Map7/Inpp4b/Ell2/Bmpr1b/Abcc4/Iqgap2
INFLAMMATORY RESPONSE	young	down	Tnfsf10/Atp2b1/Nfkbia/Il15ra/Ptger4/Slc31a1/Osmr/Nfkb1/Nlrp3/Abi1/Atp2a2/Ptger2/Tlr3/Slc4a4/Il10ra/Slc7a1/Fzd5/Clec5a/Met/Ahr/Slc28a2/Acvr1b/F3/Kcnj2/Pik3r5/Sema4d/Csf1/Il2rb/Il1a/Cd48/Cd69/Rasgrp1/Sgms2
PROTEIN SECRETION	young	down	Arfip1/Bet1/Kif1b/Gnas/Sec22b/Tmed2/Egfr/Copb2/Adam10/Atp7a/Sh3gl2/Scamp1/Ap3s1/Stam/Yipf6/Ppt1/Vps4b/Sgms1/Dop1a/Anp32e/Napg/Rab14/Arfgef2/Sec31a/Galc/Bnip3/Cln5/Dnm1l/Tpd52/Igf2r/Cav2/Mon2/Ap3b1/Arfgap3/Ap1g1/Tmx1/Stx7/Snap23/Mapk1/Lamp2/Cltc/Rps6ka3/Rab5a/Uso1/Arcn1/Clcn3/Sec24d/Copb1/Snx2/Ctsc/Stx12/Ocrl/Lman1/M6pr/Arfgef1/Golga4/Tom1l1
ALLOGRAFT REJECTION	young	down	Gzmb/Tpd52/Ccr2/Eif3a/Elf4/Ccnd2/Bcl10/Ets1/Brca1/Nlrp3/Abi1/Ube2d1/Ly75/Itk/Gcnt1/Tlr3/Irf8/Cd247/Fyb/Ccr5/St8sia4/Fgr/Cd96/Il2

			7ra/Il12rb1/Gpr65/Fasl/Ptprc/Itgb2/Csf1/Il2rb/Jak2/Ncr1/Cd28/Itgal/Il2ra/Tgfb2
WNT BETA CATENIN SIGNALING	young	down	Gnai1/Ptch1/Rbpj/Numb/Hey2/Ccnd2/Adam17/Ncstn/Notch1/Fzd1/Lef1/Ctnnb1/Jag1
KRAS SIGNALING UP	young	down	Cbl/Prrx1/Etv5/Dnmbp/Gfpt2/Ammecr1/Emp1/Ccnd2/Adam17/Ptprr/Ero1a/Ets1/Cfh/Strn/Lat2/Laptm5/Crot/F2rl1/Tspan7/Rabgap1l/Avl9/Adgra2/Trib2/Birc3/Pecam1/Gucy1a1/Lcp1/Irf8/Dusp6/Il10ra/Id2/Il33/Adamdec1/Klf4/Tnfaip3/Traf1/Mycn/Map7/Aldh1a2/Galnt3/Prkg2/Hsd11b1/Spp1/Itgb2/Abcb1a/Dock2/Ikzf1/Adam8
UV RESPONSE DN	young	down	Has2/Arhgef9/Gja1/Cav1/Fbln5/Scn8a/Dyrk1a/Notch2/Kit/Tjp1/Insig1/Vldlr/Irs1/Aggf1/Mta1/Grk5/Pdgfrb/Atp2c1/Igfbp5/Dab2/Pdlim5/Bhlhe40/Tent4a/Snai2/Ythdc1/Sfmbt1/Ptprm/Dlc1/Rnd3/Cdon/Efemp1/Plcb4/Smad3/Ptpn21/Col11a1/Tgfbr3/Nr3c1/Cdkn1b/Apbb2/Col1a2/Abcc1/Pias3/Lamc1/Phf3/Kalrn/Scaf8/Atrx/Acvr2a/Fyn/Plpp3/Atrn/Ldlr/Cdk13/Celf2/Nek7/Nipbl/Atxn1/Atp2b1/Prkca/Zmiz1/Col5a2/Rasa2/Cdc42bpa/Nfkb1/Wdr37/Bmpr1a/Nr1d2/Pten/Gcnt1/Col3a1/Tgfbr2/Togaram1/Sipa1l1/Dlg1/Slc7a1/Add3/Met/Inpp4b/F3/Adgrl2
MITOTIC SPINDLE	young	down	Vcl/Kif1b/Cenpf/Kif15/Clip1/Itsn1/Kif3c/Ranbp9/Myh9/Arhgef11/Stau1/Ezr/Kntc1/Nf1/Tiam1/Pdlim5/Cep57/Arap3/Arhgap29/Tubgcp6/Sorbs2/Fgd4/Tubgcp3/Wasf2/Arhgap4/Pafah1b1/Sos1/Arhgef3/Als2/Cdc27/Arf6/Cntrob/Espl1/Rasal2/Cenpe/Kif11/Anln/Trio/Dlgap5/Nck1/Mid1/Rabgap1/Nusap1/Ccdc88a/Pkd2/Arhgap27/Hook3/Smc3/Kif3b/Arhgef12/Tsc1/Rab3gap1/Wasl/Pcm1/Rapgef5/Tubgcp5/Cntrl/Clasp1/Epb41l2/Lrpprc/Ppp4r2/Prc1/Lats1/Rock1/Smc4/Rasa1/Akap13/Apc/Cep192/Rasa2/Cdc42bpa/Cenpj/Abl1/Kif5b/Shroom2/Myh10/Rictor/Sptbn1/Ect2/Rapgef6/Arhgap5/Kif20b/Bub1/Abi1/Pcnt/Cd2ap/Tlk1/Dock4/Ssh2/Rhof/Top2a/Dlg1/Mid1ip1/Abr/Lmnb1/Arfgef1/Net1/Dock2/Nedd9
TNFA SIGNALING VIA NFKB	young	down	Pdlim5/Yrdc/Zc3h12a/Plau/Klf10/Bhlhe40/Tnfsf9/Ripk2/Slc16a6/Ccl2/Tnfaip6/Nfe2l2/Serpinb8/Rnf19b/Icam1/Map3k8/Tnfaip2/Smad3/Pde4b/Birc2/Sik1/Cflar/Ccnl1/Vegfa/Nfat5/Rel/Ifit2/Dnajb4/Sgk1/Tank/Cxcl10/Tiparp/Ptpre/Ccnd1/B4galt5/Plpp3/Zfp36/Ldlr/Gfpt2/Btg3/Atp2b1/Nfkbia/Il15ra/Ptger4/Slc2a3/Nfkb1/F2rl1/Gem/Birc3/Ptx3/Id2/Fosl2/Klf4/Tnfaip3/Traf1/F3/Stat5a/Plek/Nr4a3/Nr4a2/Csf1/Il1a/Jag1/Cd69/Il23a
INTERFERON GAMMA RESPONSE	young	down	Tnfsf10/Adar/Nfkbia/Il15ra/Parp14/Cfh/Gbp9/Arid5b/Nfkb1/Rapgef6/Isoc1/Pnpt1/Herc6/Casp8/Ddx60/Irf8/Il10ra/Gbp8/Helz2/Trim21/Epsti1/St8sia4/Sppl2a/Rnf213/Gbp3/Samd9l/Trim14/Plscr1/Tnfaip3/Cmpk2/Casp3/Gbp4/Il2rb/Jak2/Ido1/Cd69/Slamf7
IL2 STAT5 SIGNALING	young	down	Emp1/Hopx/Ccnd2/Tnfsf10/Itgav/Gucy1b1/Slc2a3/Lrig1/Smpdl3a/Rhoh/Rabgap1l/Lrrc8c/Cyfip1/Prkch/Furin/Slc39a8/She/Ptger2/Spred2/Irf8/Sh3bgrl2/Il10ra/Ahr/Gbp3/Plscr1/Ttc39b/Traf1/Icos/Casp3/Gpr65/Spp1/Itgae/Abcb1a/Csf1/Il2rb/Itga6/Ctla4/Cd48/Eomes/Il2ra
G2M CHECKPOINT	young	down	Tle3/Rad54l/Cenpf/Kif15/Bard1/Hif1a/Meis2/Ss18/Dmd/Odf2/Stag1/Tnpo2/Hnrnpu/Kpna2/Hnrnpd/Sfpq/Tent4a/Xpo1/Slc38a1/Ythdc1/Chek1/Hmmr/Pafah1b1/Plk4/Mcm3/Cdc27/Espl1/Rasal2/Cenpe/Kif11/Top1/Lbr/Smad3/Ctcf/Nusap1/Lig3/Prpf4b/Srsf1/Cdkn1b/Aurkb/Stil/Amd1/Ilf3/Tmpo/Srsf10/Cul5/Atrx/Hus1/Mtf2/Mad2l1/Ccnd1/Pura/Syncrip/Ccnt1/Gspt1/Ccna2/Cul3/Nup98/Wrn/Prc1/Rad21/Tfdp1/Smc4/Dkc1/Slc12a2/Srsf2/Pds5b/Cul4a/Dbf4/Smc2/Abl1/Kif5b/Rad23b/Kpnb1/Kif20b/Bub1/Dr1/Slc7a5/Arid4a/Top2a/Casp8ap2/Mcm2/Rbl1/Slc7a1/Lmnb1/Polq

Table 1 - List of upregulated and downregulated genes and their respective hallmarks, based on gene enrichment analysis.

Next, we used Gene Ontology Analysis (GO - Thomas et al., 2022) to functionally characterize gene expression changes between the age groups. Overrepresentation in differentially expressed genes of category biological processes displays similarities between age groups in downregulated genes associated with cell-cell adhesion and the immune response (regulation of cell-cell adhesion, positive regulation of cell adhesion, mononuclear cell differentiation, lymphocyte differentiation, leukocyte cell-cell adhesion, regulation of leukocyte cell-cell adhesion, T cell activation, regulation of T cell activation, regulation of lymphocyte activation). In addition, we found that the gene set upregulated in later stage in young mice, could be associated only with cell respiration (oxidative phosphorylation), whereas in old mice upregulated genes are related to hormone metabolism (hormone metabolic process, hormone biosynthetic process, regulation of hormone levels, steroid catabolic process).

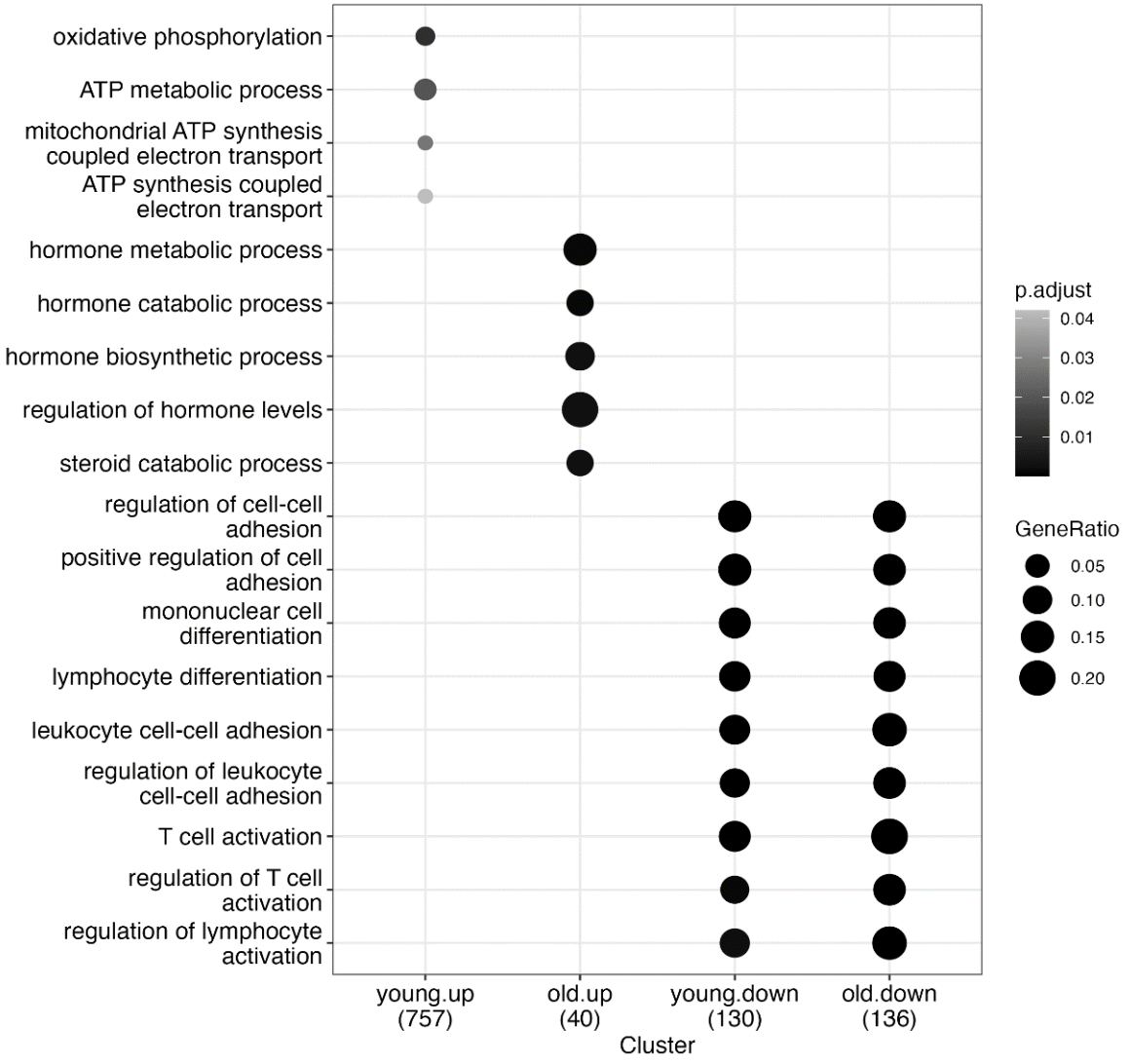

Figure 14 - Over representation of GO categories biological properties. Similarities detected in old but not young mice.

The plot of the correlation of log2 fold change shown in Figure 15, shows that statistically significantly differentially regulated genes follow a trend of change in the same direction in both age groups, but without a large overlap among genes. We have also found a number of genes that exhibit opposite patterns of expression: upregulated in young but downregulated in old mice from 15.5dpc to 17.5dpc. The correlation of temporal gene expression change between young and old mice reveals genes with contrasting expression patterns, i.e., genes that are significantly (p>0.05) upregulated from 15.5dpc to 17.5dpc in young mice, while being downregulated in old mice (upper left square of the plot shown in Figure 10).

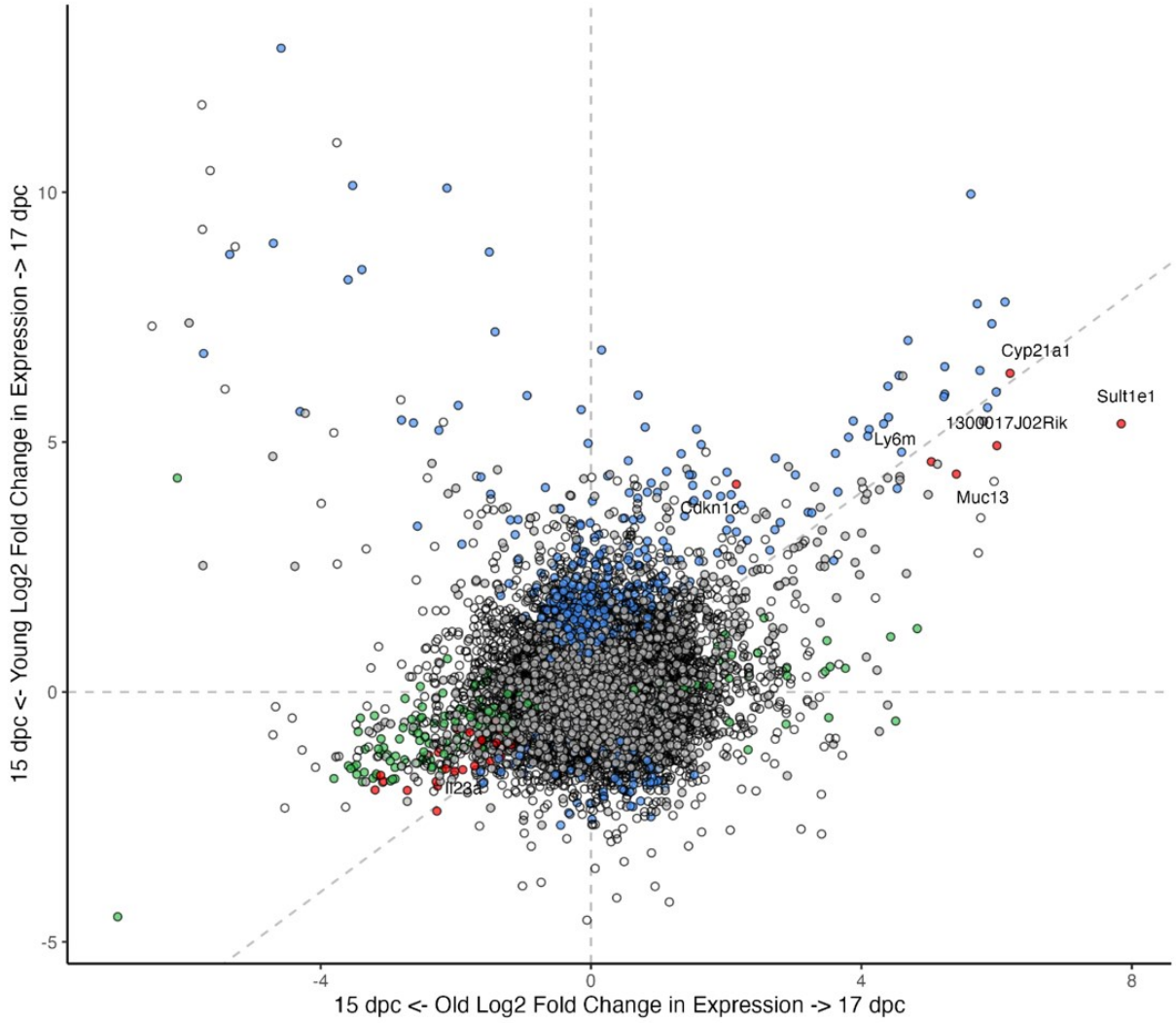

Figure 15 - Plot of correlation between the log2 fold change in the young mice (y-axis), and the log2 fold change in the old mice plotted on the x-axis. Blue data points represent significantly expressed genes in young mice, green represent significantly expressed genes in old mice, and red significantly expressed genes in both age groups. There is no obvious overlap in significantly differentially expressed genes between age groups, but genes of both age groups trend in the same direction. There is also a number of genes that are upregulated in young but downregulated in old mice.

Some of the genes that exhibit a contrasting pattern of expression between age groups are: *pregnancy-specific glycoprotein genes* (*Psg16*, *Psg17*, *Psg18*, *Psg19*, *Psg21*, *Psg22*, *Psg23*, *Psg25*, *Psg26*, *Psg27*, *Psg29*) (Figure 16), most expressed *carcinoembryonic antigen-related cell adhesion molecules* (*Ceacam3*, *Ceacam5*, *Ceacam10*, *Ceacam11*, *Ceacam12*, *Ceacam13*, *Ceacam14*, *Ceacam15*, *Ceacam16*; Figure 17), several genes encoding prolactin (*Prl2a1*, *Prl2c2*, *Prl2c3*, *Prl2c5*, *Prl3a1*, *Prl3b1*, *Prl4a1*, *Prl5a1*, *Prl7a1*, *Prl7a2*, *Prl7d1*, *Prl8a6*, *Prl8a8*, *Prl8a9*, *Prlh*) (Figure 18), *Ctsj* and *Bhlhe41*. These genes are upregulated in young and downregulated in old mice from 15.5 dpc to 17.5 dpc. The significance (p>0.05) of these dynamics is shown in Figures 16, 17 and 18.

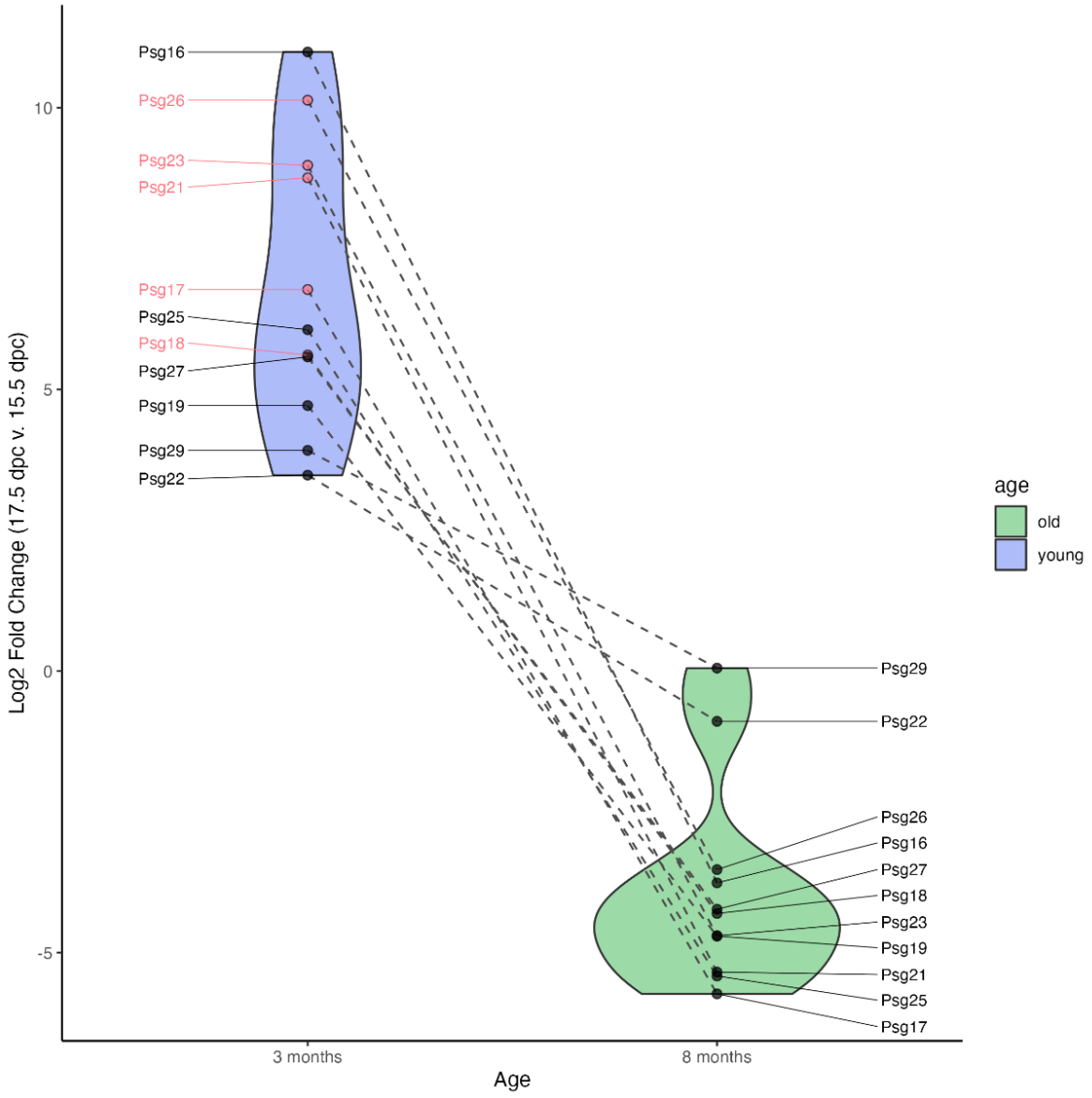

Figure 16 – *Psg* genes that are exhibiting opposite patterns of expression change from 15.5 dpc to 17.5 dpc between young (blue) and old (green) mice. Statistically significant genes are labeled red.

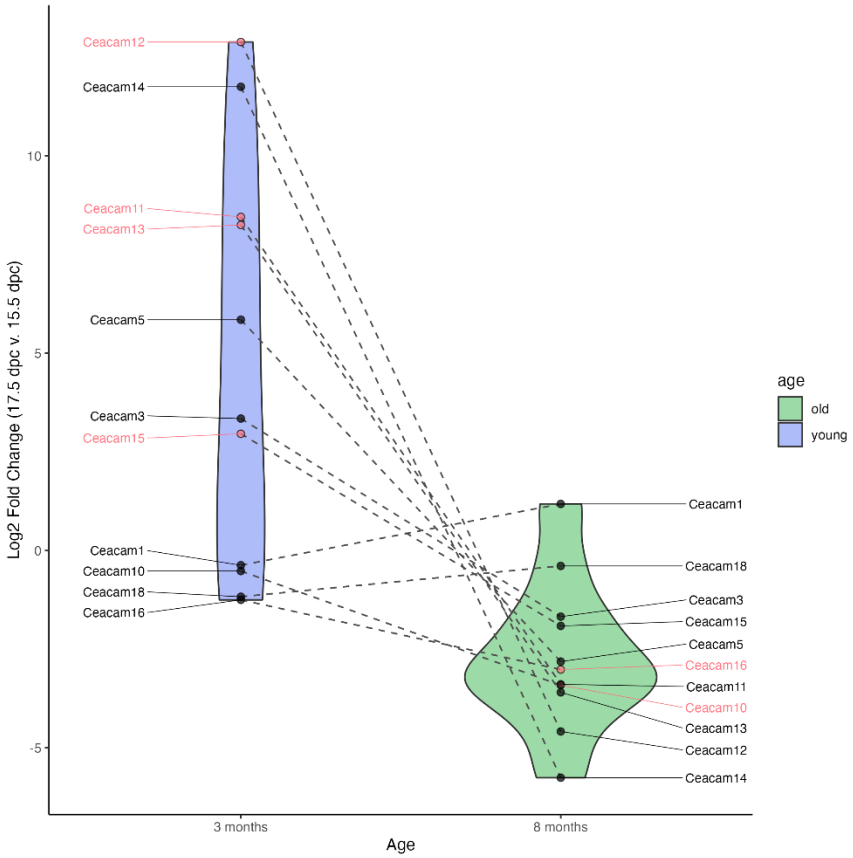

Figure 17 – *Ceacam* genes exhibiting opposite patterns of expression change from 15.5 dpc to 17.5 dpc between young (blue) and old (green) mice. Statistically significant genes are labeled red.

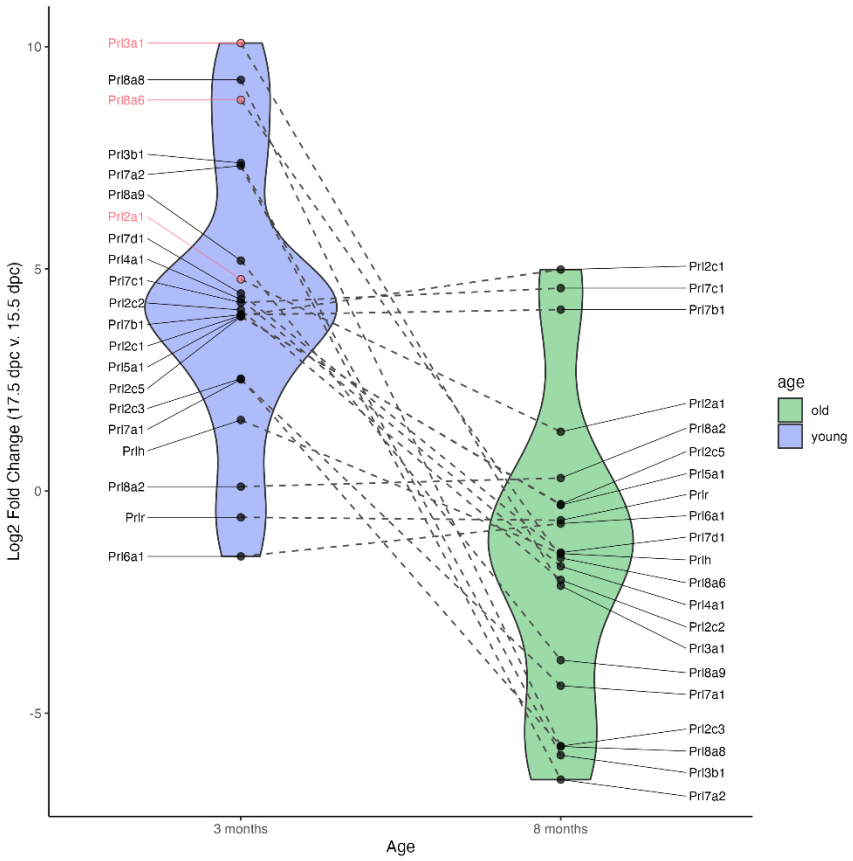

Figure 18 – *Prl* genes that are exhibiting opposite patterns of expression change from 15.5 dpc to 17.5 dpc between young (blue) and old (green) mice. Statistically significant genes are labeled red.

6. Discussion

Motivated by the established effects of aging on the gestational length and parturition in mice, this study asked about the underlying mechanisms and analyzed the effects of age on the pregnant uterus histology and transcriptome. The experiment was based on the previous observations of delayed progesterone withdrawal in (8 month) old mice, which we did not observe in our population. Somewhat surprisingly, the progesterone withdrawal in this population is apparently initiated later than in the US population of the same line studied previously. Not observing the actual decrease of progesterone levels in the young mice (3 months) at 17.5 dpc also prevented us from observing the possible delay in progesterone withdrawal in the old group. However, we did observe longitudinal changes in the uterine transcriptome which reflect the progress of pregnancy independently of observable decrease in progesterone levels, and these do show age-related effects, which may even be plausibly associated with previously reported effects of age on delayed and dystocic parturition.
The concentration of PGF2α exhibits no significant change in both young and old mice between time points. A study conducted on knockout mice that lack the prostaglandin F receptor demonstrated the importance of PGF2α signaling in luteolysis, which would eventually cause a decrease of progesterone levels. In these mice, delayed progesterone withdrawal, a consequence of failure in luteolysis, causes delayed parturition (Sugimoto et al., 1997).

Structural differences in utero-placental unit and cervix are due to pregnancy progression, not aging

Utero-placental unit at the stages of pregnancy considered here, is dominated by the fetal tissue, while the uterine decidua is very thin, where visible at all. This is no surprise, given that the mouse decidual tissue begins to deteriorate at later time points in pregnancy (from 15.5 dpc onwards), in preparation for parturition (Edwards et al., 2014). Edwards et al (2014) also reported that after 12.5 dpc, the numbers of spongiotrophoblast cells in the junctional zone increase by 4-fold, while the numbers of glycogen-containing trophoblast cells increase by 250-fold (Edwards et al., 2014). This observation is confirmed in the present study, with high abundance of glycogen-containing trophoblast cells in young mice at 15.5 dpc. Our results are thus consistent with the findings by Edwards and collaborators (2014). H&E-stained cervixes show a difference between time points, where the secretory columnar epithelia is more pronounced at 17.5 dpc, and this change occurs regardless of the age group of the animal. These results highlight the dynamic structural changes that the cervical epithelium undergoes during pregnancy, and are consistent with recent findings by Cooley and collaborators (2022).

Collagen density in the cervix

Patel and collaborators (2017) reported a decrease in collagen density throughout pregnancy in the cervical tissues of 3-, 5- and 8-months old mice. This decrease may be due to the remodeling that the cervix undergoes during late pregnancy. Prior to parturition, the cervical tissue becomes less compact, with increased presence of interstitial spaces in the extracellular matrix (Chatterjee et al., 2021). Our results confirm this for young mice, whereas the presence of interstitial spaces in the cervical stroma of the old mice is not as pronounced as in young mice, indicating a defect of tissue remodeling in old mice at 17.5 dpc.

Glycogen content in placental tissues

We found that placentas of young mice display higher levels of glycogen at 15.5 dpc, which decreases during the next two days of gestation. Old mice do not show this pattern, having low level of glycogen already at 15.5 days. The pattern in young mice is consistent with previous findings (Coan at al., 2006; Edwards et al., 2014), describing an 80-fold increase in glycogen cells from 12.5 dpc to 16.5 dpc in 6- to 8-week-old C57 BL/6J mice, followed by a notable decrease to 18.5 dpc. This pattern may be due to placental support of fetal growth during late gestation, slowly exhausting glycogen stores as a glucose source towards the end of pregnancy (Coan et al. 2006).

Transcriptomic changes during pregnancy and effects of age

Initial transcriptome analysis revealed that mice from different age groups undergo different changes in gene expression profile from early to late time points. There is also a clear difference in the number of highly expressed genes between age groups at late time point, with young mice displaying a much higher expression of significant genes, relative to old mice. There is no significant difference between young and old mice in genes that decrease in expression in late timepoint.

Genes, upregulated at the later timepoint

Among genes, upregulated at the later, relative to the earlier time point in the young mouse cohort, several processes characteristic of the transition to late pregnancy phase are enriched: coagulation, oxidative phosphorylation/ oxidative stress, DNA repair, and muscle contractility. We will in the following briefly outline some of the main processes.

Coagulation: Our findings suggest a transition of the maternal compartment towards a procoagulant state during the time of parturition. This is consistent with finding that the coagulation system undergoes changes throughout pregnancy, aimed at preventing excessive bleeding during delivery (Klaitman et al., 2013). Among the upregulated genes are those that regulate anti-coagulation (*Proc* and *Pros1*), genes involved in for-

mation of new blood vessels (*Ang*), genes that encode apolipoproteins (*Apoa1* and *Apoa4*), and matrix metalloproteinases (*Bmp1*, *Mmp7*, *Mmp10*, *Mmp11*, *Mmp15*) involved in tissue remodeling and wound healing.

Oxidative phosphorylation, oxidative stress and DNA repair: We find upregulation of these processes in young mice. This is consistent with previous reports showing that there is notable pregnancy-associated enhancement in the mitochondrial/nuclear (mt/nu) genome ratio in myometrial tissues. The process of oxidative phosphorylation relies on interaction of protein complexes in the inner mitochondrial membrane, utilizing the reduction of oxygen to generate adenosine triphosphate (ATP), which stores high-energy phosphate bonds within cells (Sunnucks et al., 2017; Deshpande & Mohiuddin, 2022). Elevated rate of this process is reflected in enhanced mitochondrial/nuclear (mt/nu) genome ratios and is frequently linked to higher rates of reactive oxygen species (ROS) generation by reverse electron flux from complex II to complex I (Quinlan et al. 2012; Dedkova et al. 2013).

Muscle contraction: Another set of upregulated genes in young cohort are genes expressed in muscle cells (*Kcnh1*, *Foxo4*, *Bdkrb2*, *Smtn*, and other) and genes related to histones, DNA damage, cell growth and apoptosis (*Hdac5*, *Gaad45b*, *Bag1*). Together this pattern may indicate a pattern of activation of uterine contractility, or tension, possibly due to fast growth of fetuses.

Effect of aging on upregulated genes

Of the above processes, it appears that age does not affect coagulation, since the genes involved in this process are upregulated in both young and old mice at 17.5 dpc, relative to 15.5 dpc. However, the old mouse cohort differs from the young mice in that we do not observe the upregulation of oxidative phosphorylation or muscle contraction.

The lack of upregulation of oxidative phosphorylation is in agreement with the previous findings on murine reproductive aging. Patel et al. (2017) have shown a clear senescence-associated reduction in the mitochondrial/nuclear (mt/nu) genome ratio DNA copy number in myometrial tissues from both pregnant and non-pregnant mice. The authors show that there is a notable pregnancy-associated enhancement in the mt/nu ratio in younger mice, whereas the enhancement is suppressed in older mice. In congruence, previous studies have shown the effect of aging on the decline of number and function of mitochondria (Wallace 1999). It appears that none of the mean activities of mitochondrial electron transport chain enzymes in the mouse myometrium are influenced by age, but the activity of succinate dehydrogenase (complex II) is enhanced only in a state of pregnancy (Patel et al., 2017). The only gene related to the complex II we identified as upregulated in young mice is *Sdhb*, a gene that provides instructions for synthesizing one of the four subunits of the succinate dehydrogenase (SDH) enzyme. Elevated activity of succinate dehydrogenase is frequently linked to higher rates of reactive oxygen species (ROS) generation by reverse electron flux from complex II to com-

plex I (Quinlan et al. 2012; Dedkova et al. 2013). The increased ROS production eventually diminishes oxidative capacities and reduces the rate of ATP synthesis (Patel et al., 2017).
During pregnancy, there is a high oxygen demand from the mother and fetus, which increases oxidative metabolism that results in generation boost of free radicals (Wisdom et al., 1991). DNA is susceptible to damage caused by ROS, and DNA damage alone results in increased levels of intracellular ROS (Evert et al., 2004; Salmon et al., 2004; Maynard et al., 2009). When not properly repaired, DNA damage can severely disrupt normal cellular functions, leading to mutations and cell death. Because of this, cells have acquired pathways to repair or respond to the presence of DNA damage (Barnes et al., 1993; Demple & Harrison 1994; Rowe et al., 2008; Maynard et al., 2009). One of the major DNA repair pathways in eukaryotic cells is nucleotide excision repair (NER). Aging studies of NER consistently demonstrated a decline of NER capacity with increasing age (Gorbunova et al., 2007). Our results are contributing to this with demonstrating upregulated expression of genes involved in NER (*Ercc1*, *Ercc2*, *Ercc8*, *Gtf2f1*, *Gtf2h5*, *Lig1*, *Ddb1*, *Rad52*) in young and their lack of expression in old mice in late timepoints.
According to the mitochondrial theory of aging (Linnane et al., 1989), a decrease in abundance of mitochondria arises as a direct result of mitochondrial ROS buildup. This in turn, leads to progressive damage to mitochondria and other cell constituents. The absence of expressed genes related to cell respiration in older mice in our transcriptome might have physiological consequences in parturition due to lower capacity for generating sufficient levels of ATP that will drive uterine contractions.

Finally, we also observe an upregulation in the old cohort of genes associated with hormone metabolism at 17.5 dpc, which was not observed in young mice.
These genes include several genes associated with steroid metabolic processes (*Cyp21a1*, *Cyp26b1*, *Cyp27b1*, *Srd5a1*, *Sult1e1*) and vitamins, ion transport, and the extracellular matrix. This may be another sign of increased inflammatory state specific to old mice, as *Cyp26b1* encodes a P450 cytochrome enzyme which degrades retinoic acid – known to promote anti-inflammatory response through Treg cells activation (Niederreitheret al., 2002; Duester et al., 2003; Bowles et al., 2006; Koubova et al., 2006; Kipp et al., 2011; Ross, 2012).

Genes, downregulated at the later timepoint
There is an extensive enrichment among downregulated genes in young mice for processes including: androgen response, WNT beta catenin signaling, protein secretion, enhanced KRAS signaling, proliferation, and an inflammatory response.

Proliferation (the cell cycle): The downregulation of genes associated with maintenance of mitotic spindle and G2M checkpoint in young mice at the late time point, may be a consequence of stalled proliferation of decidual cells. The decidua is formed *de novo* in

each pregnancy, with its life span limited by gestation length. With progressing pregnancy, the rate of proliferation of endometrial cells decreases and the rate of apoptosis of decidual cells increases, i.e. proliferation predominates apoptosis at early gestation and vice versa at late gestation (Kazakov et al., 1994; Kazakov et al. 1995; Mikhailov, 2003).
Moreover, human decidual stromal cells secrete CCL2, thereby recruiting peripheral T helper 17 cells into the decidua, which both promote proliferation and invasion of human trophoblast cells, while inhibiting apoptosis by secreting IL-17 during early pregnancy (Wu et al., 2014). Our results in young mice suggest coordinated decrease of both these functions, downregulation of proliferation as well as downregulation of genes associated with T cells in the later time point, further supporting a decreased activity of decidua.

Processes associated with androgen response: We found downregulation of genes associated with androgen response in young mice at 17.5 dpc. This is consistent with downregulation of androgen receptors from early towards late pregnancy reported before (Cheon et al., 2009; Matsumoto et al., 2013). While in female mammals, including humans, rats, and mice, the levels of androgens in blood and the uterus during estrus cycle and pregnancy are high (including dehydroepiandrosterone (DHEA), dehydroepiandrosterone sulfate (DHEAS), androstenedione (A4), testosterone (T), and dihydrotestosterone (DHT); (Kowalski et al., 2004; Cheon et al., 2009; Makieva et al., 2014), parturition is associated with decreased levels of free testosterone (Keelan et al., 2012). Similarly, androgen receptors, localized in the uterine epithelium, stroma, and myometrium (decrease mRNA and protein expression towards mid- or late-pregnancy (Pelletier et al., 2000; Weihua et al., 2002). Importantly, experimental studies using 5α-reductase-deficient mice and testicular feminized female (Tfm/Tfm) mice have revealed defects in parturition and accelerated ovarian aging (Lyon & Glenister, 1980; Mahendroo et al., 1996). Furthermore, the specific androgen antagonist hydroxyflutamide has been shown to delay implantation initiation, fetal development, and parturition in pregnant rats, as well as suppress decidualization in pseudo-pregnant rats (Chandrasekhar et al., 1990).

Effect of aging on downregulated genes
In the transcriptome of the old mice, we observed a large portion of genes associated with cell adhesion and immune response. However, genes that are involved in these processes are downregulated in young mice as well, the aging does not seem to affect the genes that become downregulated in mouse uterus during late pregnancy.

Genes with contrasting expression dynamics between age groups
CEA genes: We have also found the opposite patterns of temporal expression change in a number of genes: many genes become upregulated in young and downregulated in old mice from 15.5dpc to 17.5dpc. Two pregnancy interface-specific gene families are enriched in this pattern: pregnancy-specific glycoproteins (*Psg*) and carcinoembryonic

antigen-related cell adhesion molecules (*Ceacam*). These families are subgroups of the carcinoembryonic antigen (CEA) gene family which is located on mouse chromosome 7: *Ceacam* subgroup are mainly membrane-bound genes that code for CEA and its classical cross reacting antigens, and *Psg* subgroup encode secreted proteins (Thompson et al., 1991; Zebhauser et al., 2005). Because expression of CEA genes has been found in the invasive trophoblast of species with hemochorial placentation, these genes are thought to be involved in the processes of maternal-fetal conflict (Kammerer & Zimmermann, 2010).

Even though *Psgs* had been previously associated explicitly with placental expression, we detected them in the transcriptome of the uterine tissue. This may either indicate that they are indeed expressed in the maternal tissue, or that placental cells were included in the interface, perhaps indicating the intimate spatial entangling between the maternal and fetal tissues, composed of uterine decidual cells, maternal vasculature, glycogen trophoblast cells, and spiral artery-associated trophoblast giant cells (Panja & Paria, 2021). The expression pattern of *Psg* genes we found in young mice is consistent with literature (McLellan et al., 2005). Due to the lack of functional studies in this gene families, it is difficult to know whether the observed dysregulation in old mice has consequences for pregnancy and parturition.

Also, most members of the *Ceacam* gene family tend to increase expression in pregnancy in young and decrease it in old mice. This gene family has been associated with a regulatory role in immune tolerance during pregnancy (Mach et al., 2017), but our knowledge of individual *Ceacam* genes is not vast. Therefore, more research is needed in order to unravel the roles that these genes play in pregnancy and parturition.

Prolactin genes: Also, the expression of prolactin genes decreases in old, while increasing in young mice in late pregnancy. Prolactin is known to be synthetized locally in uterus and placenta, as extrapituitary prolactin (Bao et al., 2007, James Cross's papers), although the large majority of circulating prolactin is produced by the lactotrophic cells of the anterior pituitary. Decidual prolactin has been proposed to have an active role in functional and morphological changes in the decidua from implantation to parturition (Jabbour & Critchley, 2001; Goffin et al., 2002). Prolactins are sustaining progesterone production from the corpus luteum during pregnancy in rodents by repressing the expression of IL-6 and 20α-HSD in the decidua, and absence of this hormone affects the ability of progesterone to sustain pregnancy (Bao et al., 2007). Our results of differentially expressed prolactin genes in the mouse decidua are complementing previous studies that describe expression of these genes in the tissues of reproductive organs, such as decidua of rats and humans (Prigent-Tessier et al., 1999) and human myometrium (Bonhoff & Gellersen, 1996). However, it is not clear whether and how the changed expression in old mice may be contributing to the prolonged gestation phenotype.

Interestingly, expression of genes that encode prolactin has been detected in glycogen trophoblast cells. It has been proposed that glycogen in the placenta may provide energy for hormone synthesis from locally expressed genes such as *Prl* and *Psg* genes (McLellan et al., 2005; Simmons et al., 2008; Tunster et al., 2020). Higher glycogen levels in young mice as opposed to old mice, could thus be associated with contrasting expression pattern of *Prl* and *Psg* genes. This question would need a separate analysis in the future.

7. Conclusion

This study provides compelling evidence for the impact of female reproductive aging on the parturition in a mouse model. Notably, older mice display differences at a molecular level, compared to younger mice. The remodeling of the cervical tissues is affected in older mice, indicated by lower abundance of interspatial spaces between the collagen fibers prior to parturition. Moreover, placentas of young mice exhibit higher glycogen content at the early time point, whereas old mice have lower glycogen levels at both time points. These observations may reflect the contrasting expression of certain genes between age groups we found in the transcriptome of the decidua. To unravel the role these genes have in initiation of parturition, more research is needed. Old mice differ from young mice in gene expression profiles, with lacking upregulation of genes associated with oxidative phosphorylation and muscle contraction. These findings demonstrate that aging impacts the expression of genes involved in processes with crucial role in pregnancy progress and parturition. Taken together, the results of this study highlight the structural and genetic changes that are a consequence of reproductive senescence in mice, underscoring the importance of further research to fully comprehend the effects of aging on pregnancy and parturition.

8. References

Bao, L.; Tessier, C.; Prigent-Tessier, A.; Li, F.; Buzzio, O.; Callegari, E. A.; Horseman N.D.; Gibori, G. Decidual Prolactin Silences the Expression of Genes Detrimental to Pregnancy, Endocrinology, Volume 148, Issue 5, 1 May 2007, Pages 2326–2334, https://doi.org/10.1210/en.2006-1643

Barnes, DE.; Lindahl, T.; Sedgwick, B. (1993) DNA repair. Curr Opin Cell Biol 5: 424–433.

Bayoumi, YH.; Behairy, A.; Abdallah, AA.; Attia, NE. Peri-parturient hypocalcemia in goats: Clinical, hematobiochemical profiles and ultrasonographic measurements of postpartum uterine involution. Vet World. 2021 Mar;14(3):558-568. doi: 10.14202/vetworld.2021.558-568. Epub 2021 Mar 2. PMID: 33935398; PMCID: PMC8076444.

Bezold, K.Y.; Karjalainen, M.K.; Hallman, M. et al. The genomics of preterm birth: from animal models to human studies. Genome Med 5, 34 (2013). https://doi.org/10.1186/gm438

Bonhoff, A.; Gellersen, B. Prolactin gene expression in human myometrial smooth muscle cells is induced by cyclic adenosine 3',5'-monophosphate. Endocrine. 1996 Dec;5(3):241-6. doi: 10.1007/BF02739056. PMID: 21153074.

Bowles, J.; Knight, D.; Smith, C.; Wilhelm, D.; Richman, J.; Mamiya, S.; Yashiro, K. Chawengsaksophak K, Wilson MJ, Rossant J, Hamada H, Koopman P. Retinoid signaling determines germ cell fate in mice. Science. 2006 Apr 28;312(5773):596-600. doi: 10.1126/science.1125691. Epub 2006 Mar 30. PMID: 16574820.

Burkholder, T.; Foltz, C.; Karlsson, E.; Linton, CG.; Smith, JM. Health Evaluation of Experimental Laboratory Mice. Curr Protoc Mouse Biol. 2012 Jun;2:145-165. doi: 10.1002/9780470942390.mo110217. Epub 2012 Jun 1. PMID: 22822473; PMCID: PMC3399545.

Chandrasekhar, Y.; Armstrong, DT.; Kennedy, TG. Implantation Delay and Anti-Deciduogenic Activity in the Rat by the Anti-Androgen, Hydroxyflutamide, Biology of Reproduction, Volume 42, Issue 1, 1 January 1990, Pages 120–125, https://doi.org/10.1095/biolreprod42.1.120

Chatterjee, A.; Saghian, R.; Dorogin, A.; Cahill, LS.; Sled, JG.; Lye, S.; Shynlova, O. Combination of histochemical analyses and micro-MRI reveals regional changes of the murine cervix in preparation for labor. Sci Rep. 2021 Mar 1;11(1):4903. doi: 10.1038/s41598-021-84036-9. PMID: 33649420; PMCID: PMC7921561.

Cheon, Y-P.; Lee, D-M.; Lee, KH. (2009). Androgen in the Uterus: A Compensator of Estrogen and Progesterone. Dev. Reprod. Vol. 13, No. 3, 133-143.

Coan, PM.; Conroy, N.; Burton, GJ.; Ferguson-Smith, AC. Origin and characteristics of glycogen cells in the developing murine placenta. Dev Dyn. 2006 Dec;235(12):3280-94. doi: 10.1002/dvdy.20981. PMID: 17039549.

Cooley, A.; Madhukaran, S.; Stroebele, E.; Colon Caraballo, M.; Wang, L.; Akgul, Y.; Hon, GC.; Mahendroo, M. Dynamic states of cervical epithelia during pregnancy and epithelial barrier disruption. iScience. 2023 Jan 12;26(2):105953. doi: 10.1016/j.isci.2023.105953. PMID: 36718364; PMCID: PMC9883190.

Cornelius, AJ.; Moxon,R.; Russenberger, J.; Havlena, B.; Cheong, SH. Identifying risk factors for canine dystocia and stillbirths. Theriogenology. 2019 Apr 1;128:201-206.
doi: 10.1016/j.theriogenology.2019.02.009. Epub 2019 Feb 8. PMID: 30784806.

Crawford, NM.; Steiner, AZ. Age-related infertility. Obstet Gynecol Clin North Am. 2015 Mar;42(1):15-25. doi: 10.1016/j.ogc.2014.09.005. Epub 2014 Dec 5. PMID: 25681837.

Dedkova, EN.; Seidlmayer, LK.; Blatter, LA. Mitochondria-mediated cardioprotection by trimetazidine in rabbit heart failure. J Mol Cell Cardiol. 2013 Jun;59:41-54. doi: 10.1016/j.yjmcc.2013.01.016. Epub 2013 Feb 4. PMID: 23388837; PMCID: PMC3670593.

Demple, B.; Harrison, L. (1994) Repair of oxidative damage to DNA: enzymology and biology. Annu Rev Biochem 63: 915–948

Deshpande, OA.; Mohiuddin, SS. Biochemistry, Oxidative Phosphorylation. 2022 Aug 1. In: StatPearls [Internet]. Treasure Island (FL): StatPearls Publishing; 2023 Jan–. PMID: 31985985.

Douglas, AJ.; Leng, G.; Russell, JA. The importance of oxytocin mechanisms in the control of mouse parturition. Reproduction. 2002 Apr;123(4):543-52. doi: 10.1530/rep.0.1230543. PMID: 11914117.

Duester, G.; Mic, FA.; Molotkov, A. Cytosolic retinoid dehydrogenases govern ubiquitous metabolism of retinol to retinaldehyde followed by tissue-specific metabolism to retinoic acid. Chem Biol Interact. 2003 Feb 1;143-144:201-10. doi: 10.1016/s0009-2797(02)00204-1. PMID: 12604205.

Edwards, A.K.; Janzen-Pang, J.; Peng, A.; Tayade, C.; Carniato, A.; Yamada, A.T.; Lima, P.D.A.; Tse, D. 3 - Microscopic Anatomy of the Pregnant Mouse Uterus Throughout Gestation, Editor(s): B. Anne Croy, Aureo T. Yamada, Francesco J. DeMayo, S. Lee Adamson, The Guide to Investigation of Mouse Pregnancy, Academic Press, 2014, Pages 43-67, ISBN 9780123944450, https://doi.org/10.1016/B978-0-12-394445-0.00003-5.

Evert, B. A.; Salmon, T. B.; Song, B.; Jingjing, L.; Siede, W.; Doetsch, P. W. Spontaneous DNA damage in Saccharomyces cerevisiae elicits phenotypic properties similar to cancer cells. J. Biol. Chem. 279: 22585–22594; 2004.

Fura, M. Guinea pig dystocia in the Nordic countries – A survey study comprising Finland, Sweden, Norway, and Denmark. Degree project/Independent project, SLU Faculty of Veterinary Medicine and Animal Science, Uppsala 2022.

Gensler, HL.; Bernstein, H. DNA damage as the primary cause of aging. Q Rev Biol. 1981 Sep;56(3):279-303. doi: 10.1086/412317. PMID: 7031747.

Giller, A.; Andrawus, M.; Gutman, D.; Atzmon, G. Pregnancy as a model for aging. Ageing Res Rev. 2020 Sep;62:101093. doi: 10.1016/j.arr.2020.101093.

Goffin, V.; Binart, N.; Touraine, P.; Kelly, PA. Prolactin: the new biology of an old hormone. Annu Rev Physiol. 2002;64:47-67. doi: 10.1146/annurev.physiol.64.081501.131049. PMID: 11826263.

Gorbunova, V.; Seluanov, A.; Mao, Z.; Hine, C. Changes in DNA repair during aging. Nucleic Acids Res. 2007;35(22):7466-74. doi: 10.1093/nar/gkm756. Epub 2007 Oct 2. PMID: 17913742; PMCID: PMC2190694.

Herington, JL.; O'Brien, C.; Robuck, MF.; Lei, W.; Brown, N.; Slaughter, JC.; Paria, BC.; Mahadevan-Jansen, A.; Reese, J. Prostaglandin-Endoperoxide Synthase 1 Mediates the Timing of Parturition in Mice Despite Unhindered Uterine Contractility. Endocrinology. 2018 Jan 1;159(1):490-505. doi: 10.1210/en.2017-00647. PMID: 29029054; PMCID: PMC5761592.

Holinka, CF.; Tseng, YC.; Finch, CE. Prolonged gestation, elevated preparturitional plasma progesterone and reproductive aging in C57BL/6J mice. Biol Reprod. 1978 Nov;19(4):807-16. doi: 10.1095/biolreprod19.4.807. PMID: 570431.

Holinka, CF.; Tseng, YC.; Finch, CE. Reproductive aging in C57BL/6J mice: plasma progesterone, viable embryos and resorption frequency throughout pregnancy. Biol Reprod. 1979 Jun;20(5):1201-11. doi: 10.1095/biolreprod20.5.1201. PMID: 476251.

Jabbour, HN.; Critchley, HO. (2001). Potential roles of decidual prolactin in early pregnancy. in Reproduction. Volume 121: Issue 2. 197–205. https://doi.org/10.1530/rep.0.1210197

Kammerer, R., Zimmermann, W. Coevolution of activating and inhibitory receptors within mammalian carcinoembryonic antigen families. BMC Biol 8, 12 (2010). https://doi.org/10.1186/1741-7007-8-12

Kazakov, V. I.; Bozkov, V. M.; Linde, V. A.; and Mikhailov, V. M. (1994). Extracellular DNA in the sera of pregnant women. Cell Biol. Int. 18, 527.

Kazakov, V. I.; Bozkov, V. M.; Linde, V. A.; Repina, M. A.; and Mikhailov, V. M. (1995). Extracellular DNA in the blood of pregnant woman. Cytology (Russ.) 37, 232–236.

Keelan, JA.; Mattes, E.; Tan, H.; Dinan, A.; Newnham, JP.; Whitehouse, AJ.; Jacoby, P.; Hickey, M. Androgen concentrations in umbilical cord blood and their association with maternal, fetal and obstetric factors. PLoS One. 2012;7(8):e42827. doi: 10.1371/journal.pone.0042827. Epub 2012 Aug 20. PMID: 22916165; PMCID: PMC3423422.

Kipp, JL.; Golebiowski, A.; Rodriguez, G.; Demczuk, M.; Kilen, SM.; Mayo, KE. Gene expression profiling reveals Cyp26b1 to be an activin regulated gene involved in ovarian granulosa cell proliferation. Endocrinology. 2011 Jan;152(1):303-12. doi: 10.1210/en.2010-0749. Epub 2010 Nov 17. PMID: 21084447; PMCID: PMC3033060.

Klaitman, V; Beer-Wiesel, R; Rafaeli, T; Mazor, M; Erez, O. The Role of the Coagulation System in Preterm Parturition [Internet]. Preterm Birth. InTech; 2013. Available from: http://dx.doi.org/10.5772/54843

Koubova, J.; Menke, DB.; Zhou, Q.; Capel, B.; Griswold, MD.; Page, DC. Retinoic acid regulates sex-specific timing of meiotic initiation in mice. Proc Natl Acad Sci U S A. 2006 Feb 21;103(8):2474-9. doi: 10.1073/pnas.0510813103. Epub 2006 Feb 6. PMID: 16461896; PMCID: PMC1413806.

Kowalski, AA.; Vale-Cruz, DS.; Simmen, FA.; Simmen, RC. Uterine androgen receptors: roles in estrogen-mediated gene expressionand DNA synthesis. Biol Reprod. 2004 May;70(5):1349-57. doi: 10.1095/biolreprod.103.024786. Epub 2004 Jan 7. PMID: 14711790.

Linnane, AW.; Marzuki, S.; Ozawa, T.; Tanaka, M. Mitochondrial DNA mutations as an important contributor to ageing and degenerative diseases. Lancet. 1989 Mar 25;1(8639):642-5. doi: 10.1016/s0140-6736(89)92145-4. PMID: 2564461.

López-Otín, C.; Blasco, MA.; Partridge, L.; Serrano, M.; Kroemer, G.The hallmarks of aging. Cell. 2013 Jun 6;153(6):1194-217. doi: 10.1016/j.cell.2013.05.039.

Love, MI.; Huber, W.; Anders, S. Moderated estimation of fold change and dispersion for RNA-seq data with DESeq2. Genome Biol. 2014;15(12):550. doi: 10.1186/s13059-014-0550-8. PMID: 25516281; PMCID: PMC4302049.

Lyon, MF.; Glenister, PH. Reduced reproductive performance in androgen-resistant Tfm/Tfm female mice. Proc R Soc Lond B Biol Sci. 1980 Jun 23;208(1170):1-12. doi: 10.1098/rspb.1980.0040. PMID: 6105650.

Mach, P.; Gellhaus, A.; Prager, S.; Moore, T.; Wennemuth, G.; Kimmig, R.; Köninger, A.; Singer, BB. Soluble CEACAM1 and CEACAM6 are differently expressed in blood serum of pregnant women during normal pregnancy. Am J Reprod Immunol. 2017 Oct;78(4). doi: 10.1111/aji.12700. Epub 2017 Jun 8. PMID: 28593707.

Mahendroo, MS.; Cala, KM.; Russell, DW. 5 alpha-reduced androgens play a key role in murine parturition. Mol Endocrinol. 1996 Apr;10(4):380-92. doi: 10.1210/mend.10.4.8721983. PMID: 8721983.

Makieva, S.; Saunders, PT.; Norman, JE. Androgens in pregnancy: roles in parturition. Hum Reprod Update. 2014 Jul-Aug;20(4):542-59. doi: 10.1093/humupd/dmu008. Epub 2014 Mar 18. PMID: 24643344; PMCID: PMC4063701.

Matsumoto, T.; Sakari, M.; Okada, M.; Yokoyama, A.; Takahashi, S.; Kouzmenko, A.; Kato, S. The androgen receptor in health and disease. Annu Rev Physiol. 2013;75:201-24. doi: 10.1146/annurev-physiol-030212-183656. Epub 2012 Nov 13. PMID: 23157556.

Maynard, S.; Schurman, SH.; Harboe, C.; de Souza-Pinto, NC.; Bohr, VA. Base excision repair of oxidative DNA damage and association with cancer and aging. Carcinogenesis. 2009 Jan;30(1):2-10. doi: 10.1093/carcin/bgn250. Epub 2008 Oct 31. PMID: 18978338; PMCID: PMC2639036.

McLellan, AS.; Fischer, B.; Dveksler, G.; Hori, T.; Wynne, F.; Ball, M.; Okumura, K.; Moore, T, Zimmermann W. Structure and evolution of the mouse pregnancy-specific glycoprotein (Psg) gene locus. BMC Genomics. 2005 Jan 12;6:4. doi: 10.1186/1471-2164-6-4. PMID: 15647114; PMCID: PMC546212.

Meldrum, DR. Female reproductive aging--ovarian and uterine factors. Fertil Steril. 1993 Jan;59(1):1-5. doi: 10.1016/s0015-0282(16)55608-8.

Mikhailov, VM. (2003). Life cycle of decidual cells. Int Rev Cytol. 2003;227:1-63. doi: 10.1016/s0074-7696(03)01007-6. PMID: 14518549.

Mootha, VK.; Lindgren, CM.; Eriksson, KF.; Subramanian, A.; Sihag, S.; Lehar, J.; Puigserver, P.; Carlsson, E.; Ridderstråle, M.; Laurila, E.; Houstis, N.; Daly, MJ.; Patterson, N.; Mesirov, JP.; Golub, TR.; Tamayo, P.; Spiegelman, B.; Lander, ES.; Hirschhorn, JN.; Altshuler, D.; Groop, LC. PGC-1alpha-responsive genes involved in oxidative phosphorylation are coordinately downregulated in human diabetes. Nat Genet. 2003 Jul;34(3):267-73. doi: 10.1038/ng1180. PMID: 12808457.

Niederreither, K.; Abu-Abed, S.; Schuhbaur, B.; Petkovich, M.; Chambon, P.; Dollé, P. Genetic evidence that oxidative derivatives of retinoic acid are not involved in retinoid signaling during mouse development. Nat Genet. 2002 May;31(1):84-8. doi: 10.1038/ng876. Epub 2002 Apr 15. PMID: 11953746.

Panja, S.; Paria, BC. Development of the Mouse Placenta. Adv Anat Embryol Cell Biol. 2021;234:205-221. doi: 10.1007/978-3-030-77360-1_10. PMID: 34694483; PMCID: PMC9109784.

Patel, R.; Moffatt, JD.; Mourmoura, E.; Demaison, L.; Seed, PT.; Poston, L.; Tribe, RM. Effect of reproductive ageing on pregnant mouse uterus and cervix. J Physiol. 2017 Mar 15;595(6):2065-2084. doi: 10.1113/JP273350.

Pelletier, G.; Labrie, C.; Labrie, F. Localization of oestrogen receptor alpha, oestrogen receptor beta and androgen receptors in the rat reproductive organs. J Endocrinol. 2000 May;165(2):359-70. doi: 10.1677/joe.0.1650359. PMID: 10810300.

Pretzer, SD. Medical management of canine and feline dystocia. Theriogenology. 2008 Aug;70(3):332-6. doi: 10.1016/j.theriogenology.2008.04.031. Epub 2008 May 22. PMID: 18501414.

Prigent-Tessier, A.; Tessier, C.; Hirosawa-Takamori, M.; Boyer, C.; Ferguson-Gottschall, S.; Gibori, G. 1999 Rat decidual prolactin. Identification, molecular cloning, and characterization. J Biol Chem 274:37982–37989

Quinlan, CL.; Orr, AL.; Perevoshchikova, IV.; Treberg, JR.; Ackrell, BA.; Brand, MD. Mitochondrial complex II can generate reactive oxygen species at high rates in both the forward and reverse reactions. J Biol Chem. 2012 Aug 3;287(32):27255-64. doi: 10.1074/jbc.M112.374629. Epub 2012 Jun 11. PMID: 22689576; PMCID: PMC3411067.

Ratajczak, CK.; Muglia, LJ. Insights into parturition biology from genetically altered mice. Pediatr Res. 2008 Dec;64(6):581-9. doi: 10.1203/PDR.0b013e31818718d2. PMID: 18679156.

Rowe, LA.; Degtyareva, N.; Doetsch, PW. DNA damage-induced reactive oxygen species (ROS) stress response in Saccharomyces cerevisiae. Free Radic Biol Med. 2008 Oct 15;45(8):1167-77. doi: 10.1016/j.freeradbiomed.2008.07.018. Epub 2008 Jul 30. PMID: 18708137; PMCID: PMC2643028.

Ross, AC. Vitamin A and retinoic acid in T cell-related immunity. Am J Clin Nutr. 2012 Nov;96(5):1166S-72S. doi: 10.3945/ajcn.112.034637. Epub 2012 Oct 10. PMID: 23053562; PMCID: PMC3471201.

Salmon, T. B.; Evert, B. A.; Song, B.; Doetsch, P. W. Biological consequences of oxidative stress-induced DNA damage in Saccharomyces cerevisiae. Nucleic Acids Res. 32:3712–3723; 2004.

Sathya, A.; Prabhakar, S.; Sangha, SP.; Ghuman, SP. Vitamin E and selenium supplementation reduces plasma cortisol and oxidative stress in dystocia-affected buffaloes. Vet Res Commun. 2007 Oct;31(7):809-18. doi: 10.1007/s11259-007-0116-2. PMID: 17279464.

Simmons, D.G.; Rawn, S.; Davies, A. et al. Spatial and temporal expression of the 23 murine Prolactin/Placental Lactogen-related genes is not associated with their position in the locus. BMC Genomics 9, 352 (2008). https://doi.org/10.1186/1471-2164-9-352

Subramanian, A.; Tamayo, P.; Mootha, VK.; Mukherjee, S.; Ebert, BL.; Gillette, MA.; Paulovich, A.; Pomeroy, SL.; Golub, TR.; Lander, ES.; Mesirov, JP. Gene set enrichment analysis: a knowledge-based

approach for interpreting genome-wide expression profiles. Proc Natl Acad Sci U S A. 2005 Oct 25;102(43):15545-50. doi: 10.1073/pnas.0506580102. Epub 2005 Sep 30. PMID: 16199517; PMCID: PMC1239896.

Sugimoto, Y.; Yamasaki, A.; Segi, E,; Tsuboi, K., Aze, Y.; Nishimura, T.; Oida, H.; Yoshida, N.; Tanaka, T.; Katsuyama, M.; Hasumoto, K.; Murata, T.; Hirata, M.; Ushikubi, F.; Negishi, M., Ichikawa, A.; Narumiya, S. Failure of parturition in mice lacking the prostaglandin F receptor. Science. 1997 Aug 1;277(5326):681-3. doi: 10.1126/science.277.5326.681.

Sunnucks, P.; Morales, HE.; Lamb, AM.; Pavlova, A.; Greening, C. Integrative Approaches for Studying Mitochondrial and Nuclear Genome Co-evolution in Oxidative Phosphorylation. Front Genet. 2017 Mar 3;8:25. doi: 10.3389/fgene.2017.00025. PMID: 28316610; PMCID: PMC5334354.

Thomas, PD.; Ebert, D.; Muruganujan, A.; Mushayahama, T.; Albou, LP.; Mi, H. PANTHER: Making genome-scale phylogenetics accessible to all. Protein Sci. 2022 Jan;31(1):8-22. DOI:10.1002/pro.4218

Thompson, JA.; Grunert, F.; Zimmermann, W. Carcinoembryonic antigen gene family: molecular biology and clinical perspectives. J Clin Lab Anal. 1991;5(5):344-66. doi: 10.1002/jcla.1860050510. PMID: 1941355.

Tunster, SJ.; Watson, ED.; Fowden, AL.; Burton, GJ. Placental glycogen stores and fetal growth: insights from genetic mouse models. Reproduction. 2020 Jun;159(6):R213-R235. doi: 10.1530/REP-20-0007. PMID: 32191912.

Wallace DC. Mitochondrial diseases in man and mouse. Science. 1999 Mar 5;283(5407):1482-8. doi: 10.1126/science.283.5407.1482. PMID: 10066162.

Weihua, Z.; Ekman, J.; Almkvist, A.; Saji, S.; Wang, L.; Warner, M.; Gustafsson, J. A. (2002). Involvement of androgen receptor in 17beta-estradiol-induced cell proliferation in rat uterus. Biology of Reproduction, 67(2), 616–623. https://doi.org/10.1095/biolreprod67.2.616

Wilkinson, MJ.; Selman, C.; McLaughlin, L.; Horan, L.; Hamilton, L.; Gilbert, C.; Chadwick, C.; Flynn, JN. Progressing the care, husbandry and management of ageing mice used in scientific studies. Lab Anim. 2020 Jun;54(3):225-238. doi: 10.1177/0023677219865291. Epub 2019 Aug 12. PMID: 31403890; PMCID: PMC7301645.

Wisdom, SJ.; Wilson, R.; McKillop, JH.; Walker, JJ (1991). Antioxidant systems in normal pregnancy and in pregnancy-induced hypertension. Am J Obstet Gynecol 165: 1701–1704

Wu, HX.; Jin, LP.; Xu, B.; Liang, SS.; Li, DJ. Decidual stromal cells recruit Th17 cells into decidua to promote proliferation and invasion of human trophoblast cells by secreting IL-17. Cell Mol Immunol. 2014 May;11(3):253-62. doi: 10.1038/cmi.2013.67. Epub 2014 Mar 17. PMID: 24633013; PMCID: PMC4085486.

Yomogita, H.; Miyasaka, N.; Kanai-Azuma, M. A Review of Delayed Delivery Models and the Analysis Method in Mice. J. Dev. Biol. 2022, 10, 20. https://doi.org/10.3390/jdb10020020

Yureneva, S.; Averkova, V.; Silachev, D.; Donnikov, A.; Gavisova, A.; Serov, V.; Sukhikh, G. Searching for female reproductive aging and longevity biomarkers. Aging (Albany NY). 2021 Jun 22;13(12):16873-16894. doi: 10.18632/aging.203206. Epub 2021 Jun 22. PMID: 34156973; PMCID: PMC8266318.

Zaborski, D.; Grzesiak, W.; Szatkowska, I.; Dybus, A.; Muszynska, M.; Jedrzejczak, M. Factors affecting dystocia in cattle. Reprod Domest Anim. 2009 Jun;44(3):540-51. doi: 10.1111/j.1439-0531.2008.01123.x. Epub 2008 Nov 28. PMID: 19055561.

Zebhauser, R.; Kammerer, R.; Eisenried, A.; Mclellan, A.; Moore, T.; Zimmermann, W. 2005. Identification of a novel group of evolutionarily conserved members within the rapidly diverging murine family. Genomics 86:566–580